

Geochemical characteristics of the lower cretaceous Xiguayuan Formation mudrocks in the Luanping Basin, northern China: Implications for the hydrocarbon generation potential and sedimentary environments

Shubiao Pan^{a,b,c,d}, Zaixing Jiang^{b,*}, Yuanfu Zhang^b, Xiaodong Yuan^b, Yuhong Liao^{a,c,d,**}

^a The State Key Laboratory of Organic Geochemistry, Guangzhou Institute of Geochemistry, Chinese Academy of Sciences, Guangzhou, 510640, China

^b School of Energy Resources, China University of Geosciences (Beijing), Beijing, 100083, China

^c CAS Center for Excellence in Deep Earth Science, Guangzhou, 510640, China

^d University of Chinese Academy of Sciences, Beijing, 100049, China

ARTICLE INFO

Keywords:

Elemental geochemistry
Organic geochemistry
Hydrocarbon potential
Sedimentary environment
Luanping Basin

ABSTRACT

Thick and organic-rich mudrocks occur in the lower Cretaceous Xiguayuan Formation (K_{1x}) of the Luanping Basin, Northern China. Shale oil has been discovered for the first time in Well LT-1, adding to the oil exploration of Mesozoic hydrocarbons in the Yanshan Structural Belt. However, geochemical studies have been very limited. In this study, the core samples in Well LT-1 and several outcrop samples from stratigraphic sections were collected. Organic and inorganic geochemical analyses have been jointly carried out to study geochemical characteristics and paleoenvironments as well as the controlling factors for organic matter accumulation. The studied mudrocks are fair to excellent source rocks (total organic carbon content ~3.6 wt%). The main organic sources are aquatic plankton and terrigenous higher plants. The dominant organic matter is of type II and III. The vitrinite reflectance (0.84–1.32 %) and T_{max} values (440–467 °C) indicate mature to highly mature thermal maturity stages. The results indicate that the mudrocks have good hydrocarbon generation potential. Additionally, biomarkers and elemental composition show that they formed under anoxic lacustrine sedimentary environments with a stratified and brackish water column. The paleoclimate was semiarid, the paleoproductivity was moderate and the sedimentary rate was high. Excellent preservation and moderate productivity are the two major controlling factors for organic matter accumulation in the Xiguayuan Formation.

1. Introduction

During the mid-Cretaceous, the Yanshan Mountains experienced complex intraplate tectonic deformation and structural system transformation. As a result, many extensional superposition basins formed in the Yanshanian Structural Belt, such as the Chengde, Fengshan, Chicheng, Beipiao, and Shirengou basins (Fig. 1; Ren et al., 2002; Liu et al., 2007). Thick and organic-rich mudrocks (shales and mudstones) were deposited. The Luanping Basin is one of the typical and well-preserved basins in the Yanshan Structural Belt containing Early Cretaceous strata (Zhang et al., 2007; Cope et al., 2010). Previous studies mainly focused on sedimentological (Zhang et al., 2007; Cope et al., 2010; Jia et al., 2020; Yan et al., 2020), stratigraphical (Liu et al., 2001; Tian et al., 2008), tectonic (Wu et al., 2004) and palaeontological (Qin et al., 2017;

Xing et al., 2019) characterisations, such as those of sediment supply, Jurassic–Cretaceous boundary, dinosaur tracks and Jehol Biota fossils. However, the understanding of geochemical characteristics and sedimentary environments of the mudrocks in the lower Cretaceous Xiguayuan Formation from the Luanping Basin has been limited. Previous investigations found that the source rocks are of poor to fair hydrocarbon potential. Moreover, the volcanic activity and other tectonic movements have caused serious damage to effective reservoirs and oil and gas transportation channels (Jiao et al., 2000; Li et al., 2008).

Determining the molecular composition is useful for studying the characteristics of sedimentary organic matter (Peters et al., 2005; Hakimi et al., 2015; Ding et al., 2016). Therefore, biomarkers can effectively indicate the source of organic matter and paleoenvironmental conditions (Peters et al., 2005; Gao et al., 2018). Likewise, the

* Corresponding author.

** Corresponding author. The State Key Laboratory of Organic Geochemistry, Guangzhou Institute of Geochemistry, Chinese Academy of Sciences, Guangzhou, 510640, China.

E-mail addresses: jiangzx@cugb.edu.cn, jiangzx@cugb.edu.cn (Z. Jiang), liaoym@gig.ac.cn (Y. Liao).

<https://doi.org/10.1016/j.marpetgeo.2021.105256>

Received 12 April 2021; Received in revised form 16 July 2021; Accepted 27 July 2021

Available online 28 July 2021

0264-8172/© 2021 Elsevier Ltd. All rights reserved.

inorganic geochemical characteristics, such as the major and trace element contents of source rocks, can efficiently indicate the sedimentary environments of organic matter (Hatch and Leventhal, 1992; Worash, 2002; Cao et al., 2012). Therefore, the organic and inorganic geochemical characteristics of source rocks can provide detailed information on their hydrocarbon generation potentials and sedimentary environments.

In this study, one well was designed and drilled in the Pingfang county (named hereafter Well LT-1). It is the first hydrocarbon exploratory well in the lower Cretaceous Xiguayuan Formation (K_{1x}) in the

Luanping Basin (Fig. 1). Black thickened oil and yellowish-green light oil occurred in core samples (Fig. 2). The core samples in this well and several outcrop samples from related stratigraphic sections were selected to analyse their hydrocarbon generation potentials and sedimentary environments based on organic and inorganic geochemical data. The main objective of this study was to investigate the mechanism of organic matter enrichment in the Luanping Basin and the major controlling factors, to provide a better understanding of organic matter accumulation and a useful reference for the hydrocarbon exploration in the Yanshanian area, North China.

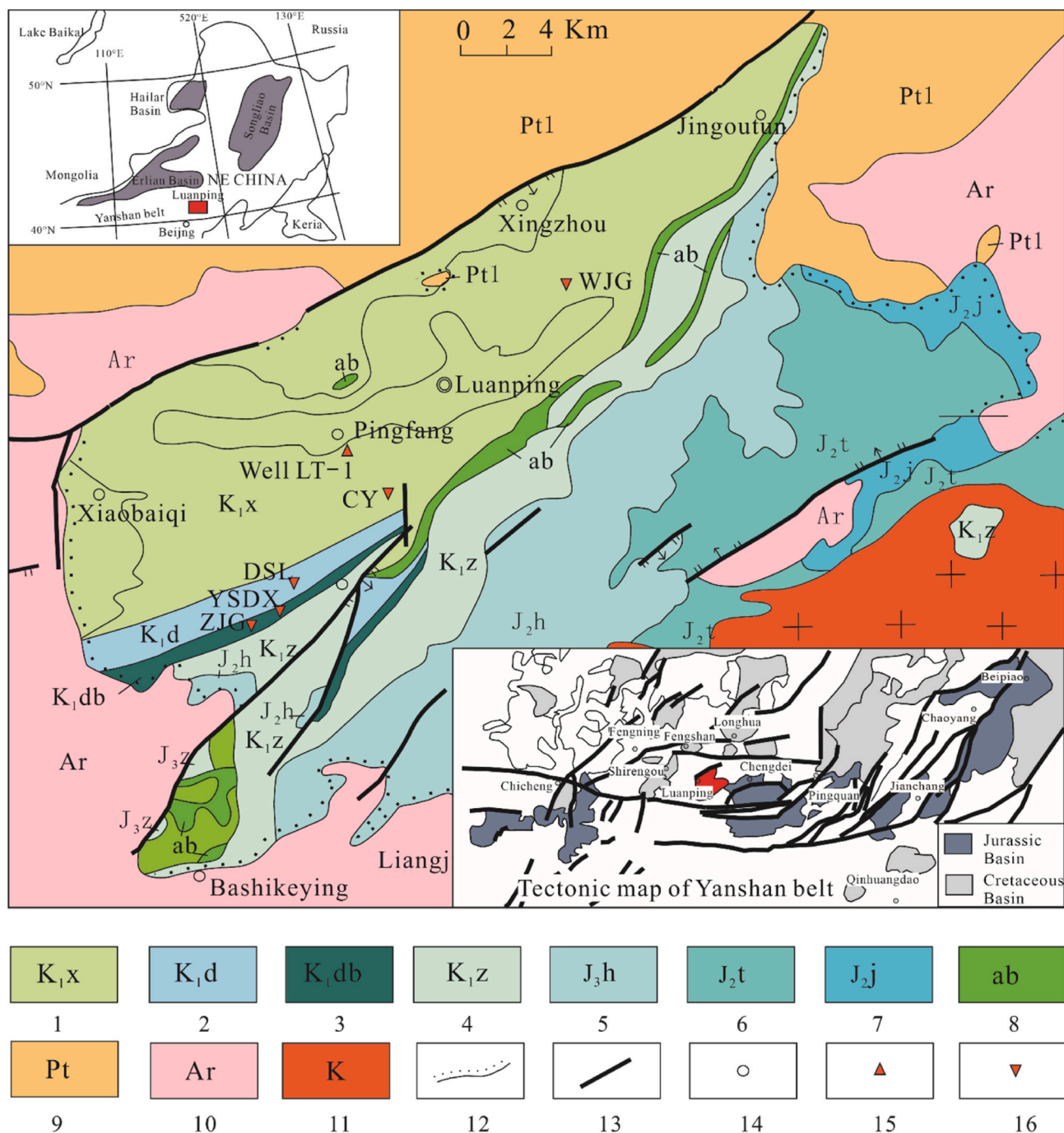


Fig. 1. Location and simplified geological map of the Luanping Basin and Yanshan Belt, showing the stratigraphic distribution, stratum dip and strike, bounding faults, and locations of the sections and Well LT-1 referred to in this study (modified from Wu et al., 2004; Qin et al., 2017). (1) Xiguayuan Formation; (2) Dadianzi Formation; (3) Dabeigou Formation; (4) Zhangjiakou Formation; (5) Houcheng Formation; (6) Tiaojishan Formation; (7) Jiulongshan Formation; (8) Andesite; (9) Proterozoic intrusive rocks; (10) Archean metamorphic rocks; (11) Cretaceous intrusive rocks; (12) unconformity boundary; (13) normal faults; (14) geographic names; (15) Well LT-1 location; (16) outcrop location. WJG: Wangjiagou Section; CY: Caoying Section.

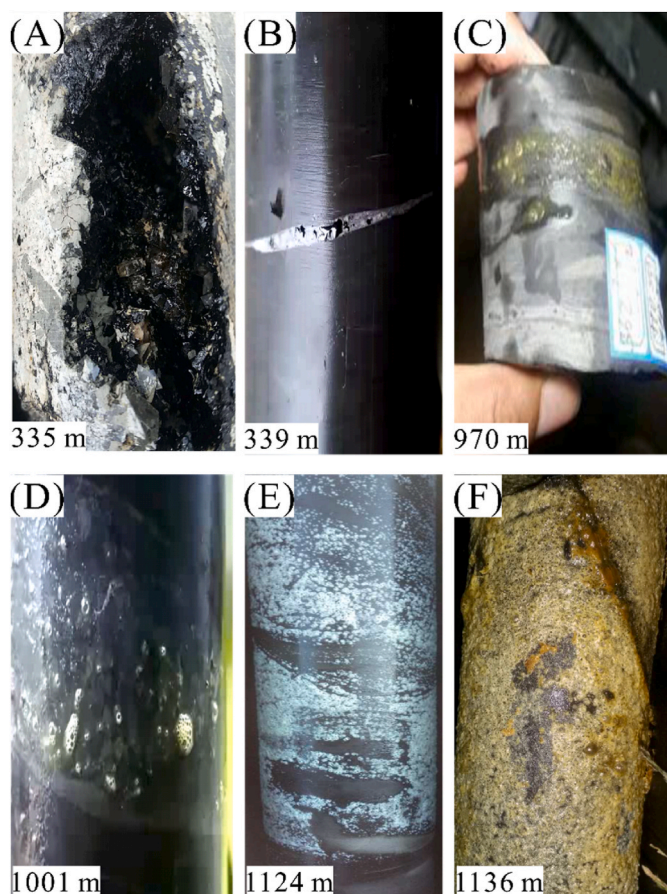


Fig. 2. Hydrocarbon within the K_{1x} core in Well LT-1, Luanping Basin. (A) Fault breccia, black thickened oil in the calcite-soluble hole at 355 m; (B) Black shale, black thickened oil at 399 m; (C) Fine-grained limestone, yellowish-green light oil at 970 m; (D) Marlstone, yellowish-green light oil at 1001 m; (E) Black mudstone, yellowish-green light oil at 1124 m; (F) Black mudstone; yellow oil fully covered the core at 1136 m. (For interpretation of the references to colour in this figure legend, the reader is referred to the Web version of this article.)

2. Geological setting

The Luanping Basin is located in the northeast of the Hebei Province, China. It is ~40 km long and 20 km wide, with a residual area of approximately 800 km² (Fig. 1). Since the Mesozoic, a series of continental volcano-faulted lake basins have formed in the North China Basin. The Luanping Basin, located in the Yanshan Structural Belt, is one of the representative and well-preserved Early Cretaceous continental volcano-faulted basins (Zhang et al., 2007). The development of the basin in the Mesozoic was mainly controlled by the Hongqi-Gangzi fault in the north and the Xiaobaiqi-Fujiadian fault in the west (Ren et al., 2002; Cope et al., 2010; Jia et al., 2020; Zhang et al., 2021).

The development of the basin included three rifting stages, namely the rift-initial, rift-climax, and rift-waning stages (Wu et al., 2004; Yan et al., 2020). Archean metamorphic rocks occur on the western and northern sides of the basin, and Yanshanian granites occur on its southeastern margin. The basement of the basin consists of Neoproterozoic metamorphic rocks and Proterozoic intrusive rocks. The formation and deposition within the Luanping Basin started in the Mesozoic. The Middle and Late Jurassic-Early Cretaceous was the main sedimentary period of the basin. The Early Cretaceous corresponds the third rifting development stage of the basin, when the lake basin area expanded to the maximum, forming an alluvial fan delta-lake sedimentary system (Li, 2003; Yuan et al., 2020, Fig. 3). The Mesozoic strata in the Luanping Basin developed from bottom to top successively, including the

Houcheng, Zhangjiakou, Dabeigou, Dadianzi and Xiguayuan formations. The thickness of the Xiguayuan Formation is ~1700 m (Wu et al., 2004; Tian et al., 2008; Yuan et al., 2020, Fig. 3).

3. Samples and methods

3.1. Samples and sections

A total of 116 core samples (black mudrock, shale, silty mudstone) were obtained from Well LT-1. Total organic carbon (TOC) and Rock-Eval analysis were performed on all samples. Using solvent extraction by column chromatography, the extract (bitumen) was separated from 38 core samples into saturated, aromatic, resin, and asphaltene (SARA) fractions, while saturated hydrocarbons were analysed by gas chromatography mass spectrometry (GC-MS). Organic petrological analysis of kerogen was performed on 23 samples. Elemental geochemical analysis was performed on 30 samples. In addition, 12 outcrop samples were acquired from two stratigraphic sections (Wangjiagou, WJG, and Caoying, CY) in the Luanping Basin. The locations of the Well LT-1 and the stratigraphic sections are indicated in Fig. 1.

The Xiguayuan Formation in the Luanping Basin is mainly composed of semi-deep lake and fan deltas facies and the volcanic events sediments (Zhang et al., 2021). The mineral components are mainly clay minerals, quartz, feldspar, calcite, and dolomite (Yuan et al., 2020). Based on lithologic composition, deposition sequence and sedimentary structure, the cores of Well LT-1 are divided into eight sections, namely PSS1–PSS4 and S_A – S_D (Fig. 4). The eight sections are divided into two parts by the conglomerate layer with a thickness of ~200 m. PSS1–PSS4 are located above the conglomerate layer, while S_A – S_D are located below the conglomerate layer.

3.2. Methods

Before the analyses, all core and outcrop samples were crushed and sieved through an 80-mesh sieve. The TOC analysis of all samples was performed with a LECO CS230 carbon-sulfur analyser. The carbonate minerals in the samples were removed with hydrochloric acid. Subsequently, these samples were burned in the oxygen-rich carrier gas at 900 °C to convert the organic carbon into carbon dioxide, after which the TOC content was measured and calculated. The basic parameters of S1 (volatile hydrocarbon content; mg HC/g rock), S2 (remaining hydrocarbon generative potential; mg HC/g rock), HI (hydrogen index; mg HC/g TOC) and T_{max} (temperature of maximum pyrolysis yield; °C) data were obtained with an OGE-II rock pyrolyser, which was developed by the Petroleum Geology Laboratory, China University of Petroleum, Beijing.

Source rock powders from 38 samples (approximately 100 g each) were extracted using a Soxhlet apparatus and chloroform for 72 h. Asphaltenes were precipitated from each Soxhlet extract by adding cold *n*-hexane, and the precipitate was filtered to obtain the asphaltene fraction. Then, each maltene fraction was divided into saturated hydrocarbons, aromatic hydrocarbons, and non-hydrocarbons using column chromatography. Furthermore, GC-MS analyses of the saturated fractions were performed with an Agilent HP6890GC/5973MSD instrument equipped with an HP-5MS fused silica column (60 m × 0.25 mm × 0.25 μm). Helium (purity 99.999 %) was introduced as a carrier gas at the flow rate of 1 mL/min via splitless injection and under an injection port temperature of 300 °C. Simultaneously, the GC oven was programmed to maintain a temperature of 50 °C for 1 min, then increase it to 120 °C at the rate of 20 °C/min, then to 310 °C at the rate of 3 °C/min, and finally to hold at 310 °C for 25 min. The mass spectrometer was operated in the electron ionisation mode at a voltage of 70 eV. The data of the biomarkers were acquired by a selective ion monitoring mode for the total ion current.

The vitrinite reflectance values (R_o , in %) were acquired following to the China National Standard GB/T 19144–2010 protocols from the


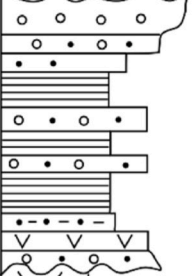

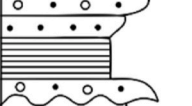
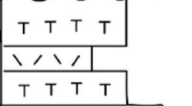
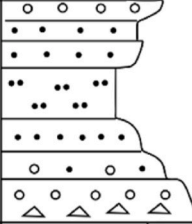
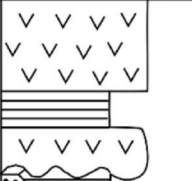
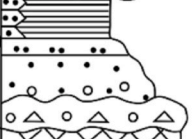

Stratigraphy		Lithologic section	Lithostratigraphy description	Sedimentary facies	Tectonic evolution
Quaternary			Modern sediments	piedmont deposit	
Lower Cretaceous (K ₁)	Xiguayuan Formation		Mainly conglomerate, sandstone, siltstone, mudstone, shale, marlite with volcanic and pyroclastic interbeds. The thickness is up to 1700 m.	alluvial fan fan delta deep and semi-deep lake	The third rifting stage
	Dadianzi Formation		Mainly conglomerate, sandstone, mudstone, shale, volcanic rock. The thickness is up to 472 m	shallow lake	
	Dabeigou Formation		Mainly conglomerate, sandstone, mudstone, shale. The thickness is up to 224 m	semi-deep, shallow lake	
	Zhangjiakou Formation		Mainly volcanics. The thickness is up to 778 m		
Upper Jurassic (J ₃)	Houcheng Formation		Mainly conglomerate, sandstone with volcanic interlayers. The maximum thickness is up to 1255 m	alluvial fan fan delta fluvial and alluvial fan	The second rifting stage
Middle Jurassic (J ₂)	Tiaojishan Formation		Mainly andesite and volcanoclastics with mudstone and sandstone interlayers. The thickness is up to 500 m		
	Jiulongshan Formation		Mainly reddish mudstone, black shale, siltstone, sandstone with underlying tuffaceous sandstone and conglomerate. The thickness is up to 224 m	shallow lake fluvial	
New Archean Group			Metamorphic rocks	Basement of the basin	



Fig. 3. Stratigraphic sequence and evolution of the sedimentary environments during different rifting stages in the Luanping Basin (revised from Qin et al., 2017; Wu et al., 2004) (1) modern sediments; (2) breccia; (3) conglomerate; (4) sandstone; (5) mudstone; (6) intermediate volcanic rocks; (7) felsic volcanic rocks; (8) rhyolite; (9) basement.

kerogen samples, which were analysed by a 308-PV microphotometer at Petroleum Geology Laboratory, China University of Petroleum, Beijing. Stable carbon isotope values of kerogen were determined for 13 core samples selected above the conglomerate in Well LT-1 and for 10 outcrop samples in the WJG surface section. The $\delta^{13}\text{C}$ analysis was performed by means of a FLASH HT EA-MAT 253 isotope ratio mass spectrometer using the SY/T 5238–2008 testing standard. Isotopic ratios

are reported in standard δ -notation and relative to the PDB standard. Major elements were analysed by AB104L, Axios_{max} X-ray fluorescence spectrometer following the China National Standard GB/T 15406.28–2010 protocols. The measurements of trace and rare earth elements (REE) were conducted using an Element XR Mass spectrometer in the Beijing Institute of Nuclear Industry Geology following the China National Standard GB/T 14506.30–2010 protocols.

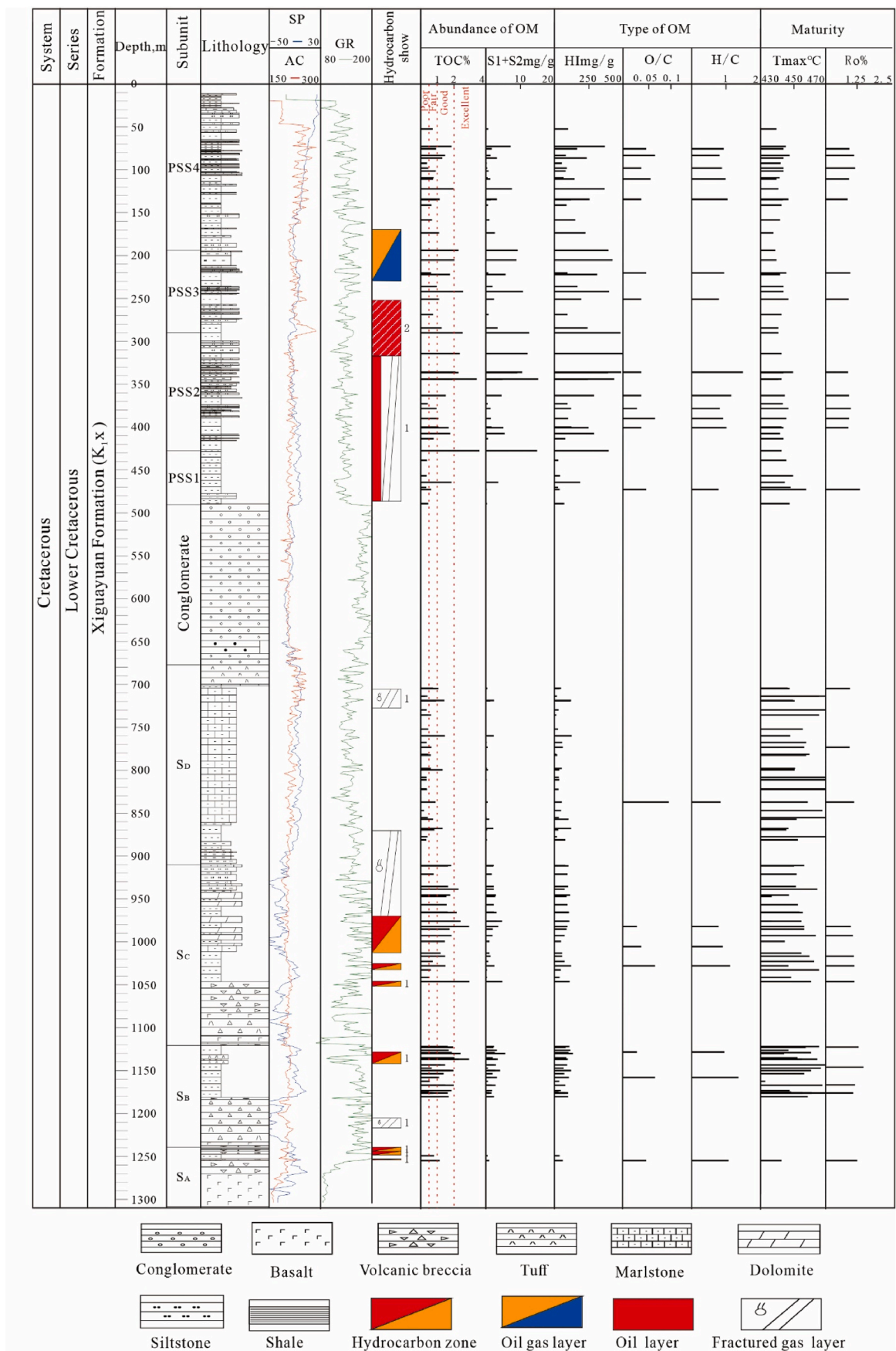


Fig. 4. Variations in abundance, type, and maturity of organic matter in the Lower Cretaceous Xiguayuan Formation core (K₁x) samples from Well LT-1 in the Luanping Basin.

4. Results

4.1. Organic geochemical characteristics

4.1.1. TOC content and Rock-Eval analysis

The wide-ranging results of the TOC and Rock-Eval analyses for the K_{1x} samples are presented in Table 1 and Fig. 4). For the core samples in the PSS2, the TOC contents range from 0.44 % to 3.60 % (mean = 1.86 %), the S_1+S_2 values from 0.50 to 15.18 mg HC/g rock (mean = 6.67 mg HC/g rock), while the HI values range from 78.42 to 498.56 mg HC/g TOC (mean = 284.43 mg HC/g TOC). In the PSS3 samples, the TOC contents range from 0.64 % to 2.56 % (mean = 1.50 %), the S_1+S_2 values from 0.71 to 10.78 mg HC/g rock (mean = 4.87 mg HC/g rock) and the HI values from 95.00 to 421.80 mg HC/g TOC (mean = 257.11 mg HC/g TOC). The TOC contents and S_1+S_2 are higher in the PSS2 and PSS3 samples compared with PSS1 (TOC content is 0.68 % on average, 0.75 mg HC/g rock S_1+S_2 on average) and PSS4 (TOC content is 1.01 % on average, 2.06 mg HC/g rock S_1+S_2 on average). For the samples below the conglomerate, the TOC contents and the S_1+S_2 values are in the ranges of 0.50–2.96 % (mean = 1.52 %) and 0.21–5.56 mg HC/g rock (mean = 2.16 mg HC/g rock) in the S_B , respectively; the TOC contents and S_1+S_2 values are in the ranges of 0.80–2.97 % (mean = 1.85 %) and 0.21–5.56 mg HC/g rock (mean = 2.52 mg HC/g rock) in the S_C , respectively. Therefore, the TOC contents and S_1+S_2 values in both S_B and S_C are higher than those in S_A (0.99 % TOC on average, 0.76 mg HC/g rock S_1+S_2 on average) and S_D (0.85 % TOC on average, 0.78 mg HC/g rock S_1+S_2 on average). According to the universal standard of hydrocarbon source rock abundance, 87 % of the mudrocks PSS2 samples and 77 % of the PSS3 samples correspond to good–excellent source rocks (TOC > 1.0 %). However, 84 % of the PSS1 mudrock samples and 65 % of the PSS4 samples correspond to poor–fair source rocks (0.5 % < TOC < 1.0 %) (Peters, 1986, Figs. 3 and 5). The TOC and Rock-Eval pyrolysis data indicate that source rocks in the S_B and S_C subunits have good to excellent potentials. Additionally, the samples in S_A mudrocks show the characteristic of fair–good source rocks, while the quality of the source rocks is poor and fair in S_D (Figs. 3 and 5).

Regarding the outcrop samples in the Luanping Basin (located in Fig. 1), in the WJG section, the TOC range from 0.31 % to 2.78 % (mean = 1.50 %), the S_1+S_2 values from 0.14 to 7.37 mg HC/g rock (mean = 2.78 mg HC/g rock) and the HI values from 29 to 584 mg HC/g TOC (mean = 171 mg HC/g TOC). As for the CY section, the related data are lower than the WJG section (only 0.48 % TOC on average, 2.78 mg HC/g rock S_1+S_2 on average). Approximately 80 % of mudrock samples in the WJG section reach the standard of good to excellent source rocks,

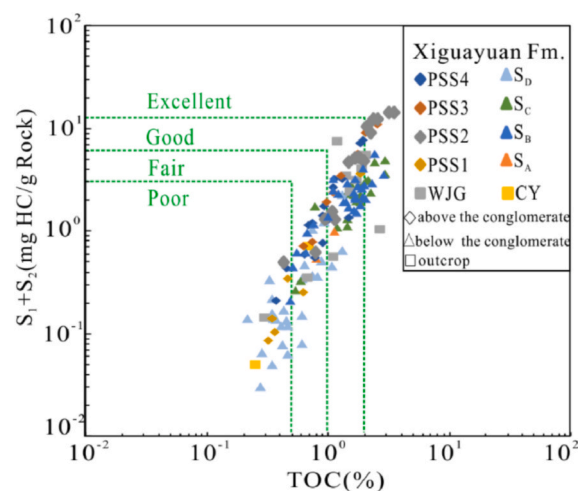


Fig. 5. Cross diagram of Rock-Eval S_1+S_2 versus TOC for the K_{1x} samples in the Luanping Basin.

whereas all samples from the CY sections reflect the characteristics of poor to fair source rocks (Fig. 5; Table 1). The quality of source rocks from the Xiguayuan Formation indicates good hydrocarbon generation potential (Fig. 5). The high-quality source rocks in the Xiguayuan Formation were mainly developed in S_B , S_C , PSS2, and PSS3 rocks.

It is worth noting that the T_{max} values for all samples show great variations in the Luanping Basin. For the K_{1x} mudrock samples in Well LT-1, the T_{max} values vary vertically. The samples above the conglomerate have T_{max} values in the 440–458 °C range (mean = 444 °C), which is lower than that of samples below the conglomerate (433–475 °C, mean = 453 °C). In the WJG and CY sections, the outcrop samples show lower T_{max} values compared with the core samples, in ranges 443–451 °C and 440–460 °C, respectively.

4.1.2. Kerogen elemental compositions

The atomic ratios of O to C (O/C) for all core samples range from 0.03 to 0.10 (mean = 0.05), while the atomic ratios of H to C (H/C) range from 0.78 to 1.49 (mean = 0.96). As for the outcrop samples from the WJG surface section, the O/C and H/C atomic ratios range widely from 0.13 to 0.21 (mean = 0.16) and from 0.89 to 1.51 (mean = 1.15), respectively.

Table 1

Partial geochemical indicators of the Lower Cretaceous source rocks in the Luanping Basin (0.38–2.00: Minimum–Maximum; 1.01 (17): Mean (Sample number)).

Formation	Sections/Well	Subunit	TOC (%)	S_1+S_2 mg/g	HI mg/g	Ro (%)	T_{max} °C	H/C	O/C
K_{1x}	LT-1	PSS4	0.38–2.00	0.21–7.58	51.82–366.7	0.84–1.13	438–448	0.81–1.04	0.04–0.07
			1.01 (17)	2.06 (17)	160.02 (17)	0.97 (5)	443 (17)	0.93 (5)	0.05 (5)
		PSS3	0.64–2.59	0.71–10.78	95.00–421.80	0.88–0.95	439–447	0.79–0.94	0.04–0.05
			1.50 (9)	4.87 (9)	257.11 (9)	0.92 (2)	443 (9)	0.86 (2)	0.05 (2)
		PSS2	0.44–3.60	0.50–15.18	78.42–498.56	0.86–0.98	441–450	0.82–1.49	0.03–0.07
			1.86 (15)	6.67 (15)	284.43 (15)	0.90 (5)	444 (15)	1.08 (5)	0.05 (5)
		PSS1	0.33–1.89	0.09–3.6	25.58–187.28	1.32 (1)	445–458	0.78 (1)	0.05 (1)
			0.68 (6)	0.75 (6)	64.78 (6)		449 (6)		
		S_D	0.34–1.46	0.15–2.30	21–124.89	0.92–1.09	446–459	0.84 (1)	0.10 (1)
			0.85 (17)	0.78 (17)	64.70 (17)	0.98 (4)	452 (17)		
		S_C	0.80–2.97	1.10–4.85	47.86–119.03	0.97–1.11	437–461	0.78–1.12	0.03–0.07
			1.85 (20)	2.52 (20)	90.10 (20)	1.06 (6)	453 (20)	0.93 (3)	0.04 (3)
		S_B	0.50–2.96	0.21–5.56	30–163.50	1.05–1.32	422–475	0.95–1.36	0.03–0.07
			1.52 (30)	2.16 (30)	90.59 (30)	1.20 (4)	455 (30)	1.15 (2)	0.05 (2)
S_A	0.82–1.16	0.53–0.99	38.66–60.40	1.21 (1)	413–443	1.07 (1)	0.05 (1)		
	0.99 (2)	0.76 (2)	49.53 (2)		428 (2)				
WJG	–	0.31–2.78	0.14–7.37	29–584	0.64–0.70	443–451	0.89–1.51	0.13–0.21	
		1.50 (10)	2.78 (10)	171 (10)	0.68 (10)	446 (10)	1.15 (10)	0.16 (10)	
CY	–	0.2–0.7	0.71–0.005	20–90	–	440–460	–	–	
		0.48 (2)	0.38 (2)	50 (2)		450 (2)			

4.1.3. Carbon isotopes in kerogen

The kerogen carbon isotopic compositions were analysed for 13 core samples, which were all obtained from 4 subunits (PSS1, PSS2, PSS3 and PSS4) above the conglomerate in Well LT-1. The kerogen carbon isotope values ($\delta^{13}\text{C}$) for the core K_{1x} samples ranged from -26.0‰ to -19.6‰ , with an average value of -22.3‰ . As for the 10 outcrop samples from the WJG surface section, the $\delta^{13}\text{C}$ values similarly ranged from -26.7‰ to -23.1‰ with an average value of -25.6‰ .

4.1.4. Vitrinite reflectance

The Ro values for the 28 core samples (including 13 samples from the PSS1, PSS2, PSS3 and PSS4 and 15 samples from S_A , S_B , S_C , S_B and S_A) range from 0.86 % to 1.32 %, with an average value of 1.00 % (Fig. 4). In particular, the Ro values for the samples above the conglomerate in PSS1, PSS2, PSS3 and PSS4 range from 0.86 % to 1.32 %, with an average value of 0.96 %, whereas those for the samples below the conglomerate in S_A , S_B , S_C , S_B and S_A have slightly higher values from 0.92 % to 1.32 %, with an average value of 1.10 %. Additionally, the Ro values for the 10 outcrop samples range from 0.64 % to 0.7 %, with an average value of 0.68 %.

4.1.5. Biomarkers

Biomarkers were analysed in the core samples collected from the Well LT-1 in the Xiguayuan Formation, because the outcrop samples had been significantly affected by weathering.

4.1.5.1. Normal alkaline and isoprenoids. The profiles of *n*-alkaline and isoprenoids are shown in Fig. 6, and the analytical parameters in Table 2. Analytical data show that the carbon numbers of *n*-alkanes in the Lower Cretaceous Xiguayuan Formation core samples range from *n*- C_{13} to *n*- C_{35} . Most samples below the conglomerate mainly show a unimodal distribution with *n*- C_{19} major *n*-alkanes and exhibit a C_{21}^-/C_{22}^+ ratio higher than 1. However, the samples above the conglomerate show a weak bimodal pattern between *n*- C_{17} and *n*- C_{23} , with a C_{21}^-/C_{22}^+ ratio lower than 1. The terrigenous to aquatic ratio (TAR) values are consistent with the C_{21}^-/C_{22}^+ ratio. The carbon predominance index (CPI) and the odd-even predominance (OEP) value of nearly all core samples range from 1.04 to 1.46 (mean = 1.21) and from 0.94 to 1.15 (mean = 1.05), respectively, indicating a weak odd-carbon predominance. However, a few samples below the conglomerate show a slight even-carbon predominance with the OEP lower than 1 (Table 2). There is a light-end

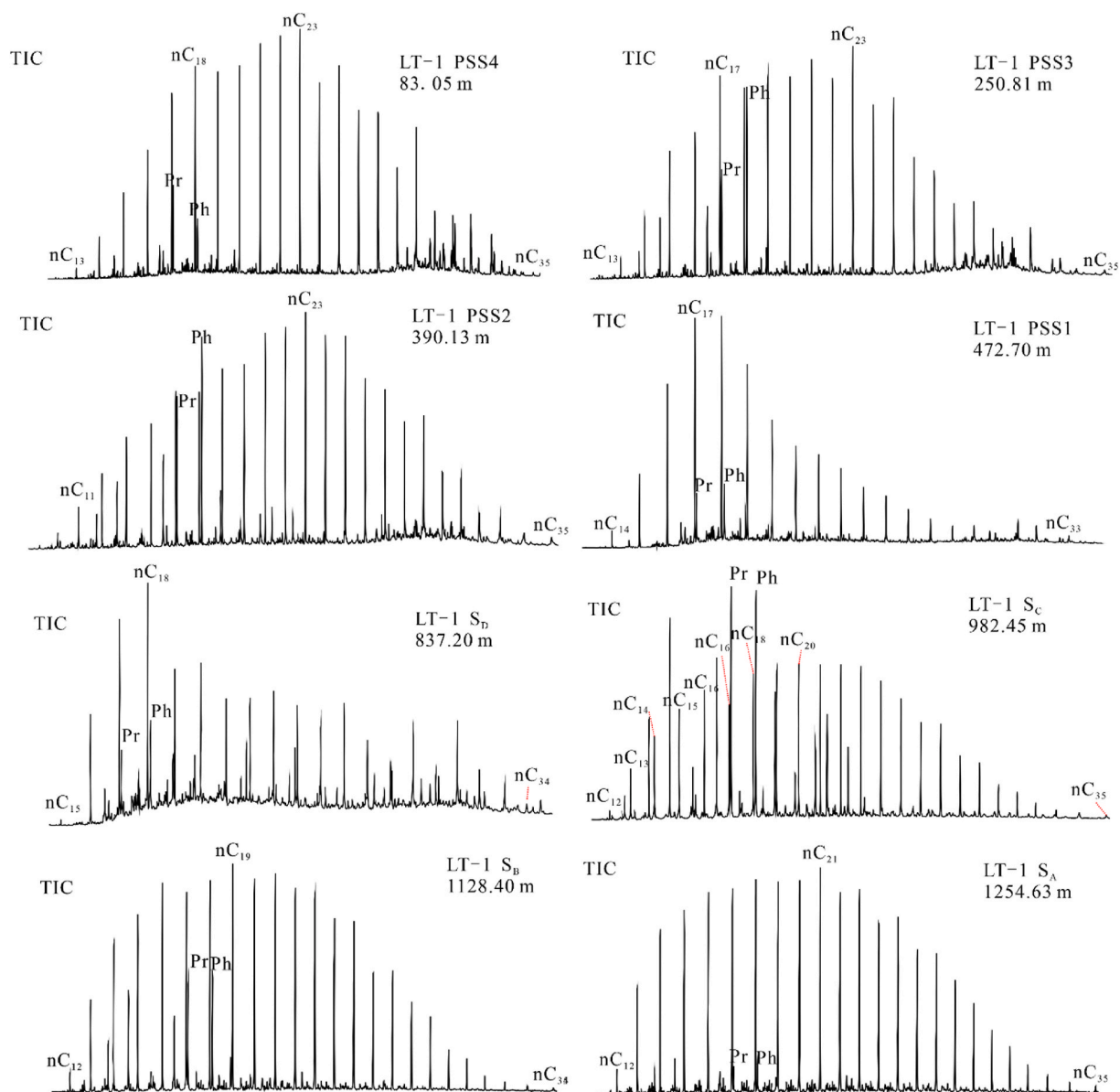


Fig. 6. Total ion chromatograms (TIC) plots of saturated hydrocarbon fractions from core samples of the Xiguayuan Formation in the Luanping Basin.

Table 2

Normal alkanes and isoprenoids for K_1x samples in Well LT-1 from the Luanping Basin ($CPI = [(C_{25} + C_{27} + C_{29} + C_{31} + C_{33}) / (C_{24} + C_{26} + C_{28} + C_{30} + C_{32}) + (C_{25} + C_{27} + C_{29} + C_{31} + C_{33}) / (C_{26} + C_{28} + C_{30} + C_{32} + C_{34})] / 2$, after Bray and Evans (1961); $OEP = [(C_{i+6} \times C_{i+2} + C_{i+4}) / (4 \times C_{i+1} + 4 \times C_{i+3})]^m$, $m = (-1)^{i+1}$; $i+2$ denotes main peak carbon number of n -alkanes, after Scalan and Smith (1970); C_{21}^- represents carbon number less than C_{21} ; C_{22}^+ represents carbon number greater than C_{22} respectively; $TAR = (C_{27} + C_{29} + C_{31}) / (C_{15} + C_{17} + C_{19})$, after Bourbonniere and Meyers (1996)).

Formation	Subunit	Depth, m	Major Alkanes	CPI	OEP	C_{21}^-/C_{22}^+	TAR	Pr/ n - C_{17}	Ph/ n - C_{18}	Pr/Ph
K_1x	PSS4	75.50	23	1.41	1.13	0.84	0.59	0.95	2.02	0.54
		83.05	23	1.39	1.08	0.67	1.00	0.84	0.49	1.54
		97.80	23	1.32	1.05	0.59	1.03	2.01	1.79	1.02
		110.98	23	1.46	1.09	0.73	0.64	2.29	3.63	0.65
	PSS3	134.33	23	1.37	1.15	0.75	0.75	0.89	2.40	0.38
		220.55	23	1.38	1.08	0.58	1.27	0.94	0.80	1.14
		250.81	23	1.25	1.10	0.92	0.49	0.83	1.79	0.49
		336.00	23	1.23	1.09	0.49	1.25	1.39	2.69	0.41
	PSS2	363.30	23	1.24	1.09	0.77	0.66	1.26	2.38	0.49
		378.52	23	1.23	1.05	0.65	0.94	1.48	1.42	0.99
		390.13	23	1.26	1.06	0.65	0.94	1.52	2.30	0.64
		400.90	23	1.12	1.03	0.66	0.71	2.49	4.29	0.57
	PSS1	472.70	17	1.22	1.03	2.62	0.14	0.35	0.44	0.80
		773.30	23	1.07	1.02	0.43	2.48	1.08	0.75	0.65
	S_D	837.20	23	1.20	1.08	0.58	1.59	0.83	0.61	0.73
		921.15	19	1.14	0.94	1.46	0.67	4.02	2.86	1.73
	S_C	982.45	19	1.13	1.06	1.42	0.49	3.30	2.15	1.42
		992.85	19	1.12	1.04	1.08	0.64	2.39	1.57	1.39
		1016.65	19	1.10	1.03	0.94	0.68	2.07	1.21	1.61
		1028.20	19	1.20	1.03	0.95	0.63	0.43	0.59	0.66
		1041.50	19	1.11	1.03	0.80	0.81	1.28	0.48	2.29
		1122.88	19	1.04	1.02	1.22	0.39	0.55	0.58	0.91
		1128.40	19	1.18	1.00	1.44	0.31	0.64	0.70	0.89
	S_B	1129.80	20	1.14	1.00	1.08	0.49	0.47	0.60	0.72
		1136.70	19	1.14	1.00	1.23	0.41	0.38	0.60	0.59
		1157.88	19	1.07	1.01	1.16	0.48	0.77	0.75	0.97
		1254.63	21	1.11	0.99	1.20	0.42	0.11	0.15	0.74

truncation in some samples (Fig. 6), which could be attributed to weathering, biodegradation, and high maturity (Peters et al., 2005). However, considering that the test samples are selected from a freshly drilled core, the influence of weathering can be ignored. The unresolved complex mixtures and 25-norhopanes, indicator of biodegradation, were not commonly detected in all the measured samples. Therefore, the differences in thermal maturity of the source rocks may be the most reasonable factor affecting the distributions of alkanes and isoprenoids. Due to the effect of evaporation loss, the C_{21}^-/C_{22}^+ values in this study might be lower than the original values (Cao et al., 2018).

According to Table 2, the pristane/phytane (Pr/Ph) ratios of all samples in Well LT-1 range from 0.41 to 2.29, with an average value of 0.92. In general, the Pr/Ph ratios for the samples above the conglomerate (mean = 0.74) are lower than those for the samples below the conglomerate (mean = 1.09) (Table 2). The Pr/ n - C_{17} and Ph/ n - C_{18} ratios denote the ratio of isoprenoids to the adjacent n -alkanes. The Pr/ n - C_{17} and Ph/ n - C_{18} ratios of all K_1x core samples range from 0.15 to 4.29 (mean = 1.45) and from 0.11 to 7.03 (mean = 1.37), respectively.

4.1.5.2. Steranes. Regular steranes C_{27} – $C_{29}\alpha\alpha\alpha$ and diasteranes C_{27} – C_{29} were identified in the $m/z = 217$ mass fragmentograms (Fig. 7). The relative abundance of C_{27} , C_{28} and C_{29} regular steranes show vertical variations in the K_1x samples from Well LT-1 (Fig. 7; Table 3). Regarding the samples above the conglomerate in Well LT-1, the samples from the PSS4 show a weak higher proportion of C_{29} (29.56–51.29 %) compared to C_{27} (23.58–47.15 %) and C_{28} (15.12–22.59 %) with anti-L shape on the fragmentograms. In contrast, for the remaining three subunits (PSS1, PSS2, and PSS3), the relative abundance of C_{29} , C_{28} and C_{27} are in the ranges of 22.76–45.66 % (mean = 35.88 %), 13.89–23.58 % (mean = 19.19 %) and 30.92–53.76 % (mean = 44.42 %), respectively. Most samples show the distribution of $C_{27} > C_{29} > C_{28}$ and a typical L-shape, while less samples show $C_{27} \approx C_{29} > C_{28}$ on the sterane fragmentograms. As for the samples below the conglomerate in Well LT-1, the $C_{29}\alpha\alpha\alpha$ (20R)/ $C_{27}\alpha\alpha\alpha$ (20R) and the $C_{28}\alpha\alpha\alpha$ (20R)/ $C_{27}\alpha\alpha\alpha$ (20R) range from 0.35 to 2.17 (mean = 1.20) and from 0.30 to 0.86 (mean = 0.59),

respectively. And the distribution of C_{27} – C_{29} regular steranes show the clear feature of $C_{29} > C_{27} > C_{28}$ with the reverse L-shape on the mass fragmentograms.

The C_{29} sterane isomerization parameters [$C_{29}\alpha\alpha\alpha$ 20S/(20S + 20R) and $C_{29}\alpha\beta\beta/(\alpha\beta\beta + \alpha\alpha\alpha)$] show a slight variation vertically in the K_1x samples from Well LT-1 (Fig. 7; Table 3). The mudrock samples above the conglomerate have a $C_{29}\alpha\alpha\alpha$ 20S/(20S + 20R) ratio in the 0.38–0.50 range (mean = 0.45) and a $C_{29}\alpha\beta\beta/(\alpha\beta\beta + \alpha\alpha\alpha)$ ratio in the 0.39–0.59 range (mean = 0.50), while the core samples below the conglomerate show a $C_{29}\alpha\alpha\alpha$ 20S/(20S + 20R) ratio in the 0.34–0.55 range (mean = 0.48) and a $C_{29}\alpha\beta\beta/(\alpha\beta\beta + \alpha\alpha\alpha)$ ratio in the 0.37–0.58 range (mean = 0.52).

4.1.5.3. Terpanes. The $m/z = 191$ ion chromatograms, indicating the distribution and relative abundance of tricyclic terpanes and pentacyclic terpanes (hopanes), are presented in Fig. 7 and Table 3. Tricyclic terpanes, ranging from C_{19} to C_{29} , were identified in most samples. Regarding the samples above the conglomerate in Well LT-1, the distributions of related tricyclic terpanes are characterised by $C_{23} > C_{21} > C_{20}$ or $C_{21} > C_{23} > C_{20}$. As for the samples below the conglomerate in Well LT-1, the C_{20}/C_{23} and C_{21}/C_{23} tricyclic terpane ratios range from 0.45 to 1.96 (mean = 0.84) and from 0.69 to 1.27 (mean = 0.86), respectively, implying that the samples follow an order of $C_{23} > C_{21} > C_{20}$ (Fig. 7).

The distribution of triterpanes (hopanes) is presented in Fig. 7. The $C_{30} \alpha\beta$ hopane is predominant in almost all the investigated samples (Fig. 7). The Ts (18 α (H)-22, 29, 30-trinorhopane)/Tm (17 α (H)-22, 29, 30-trinorhopane) ratios of the samples above the conglomerate range from 0.25 to 2.48 (mean = 0.88), which are generally higher than those below the conglomerate (0.4–1.12, mean = 0.72).

Gammacerane was detected in some samples from the Well LT-1 core (Fig. 7). The gammacerane index (GI), defined as gammacerane/ $C_{30} \alpha\beta$ hopane ratio, is in the 0.08–0.80 range of values (mean = 0.43) for the samples above the conglomerate. Whereas the samples below the conglomerate have lower values from 0.16 to 0.28, with an average GI

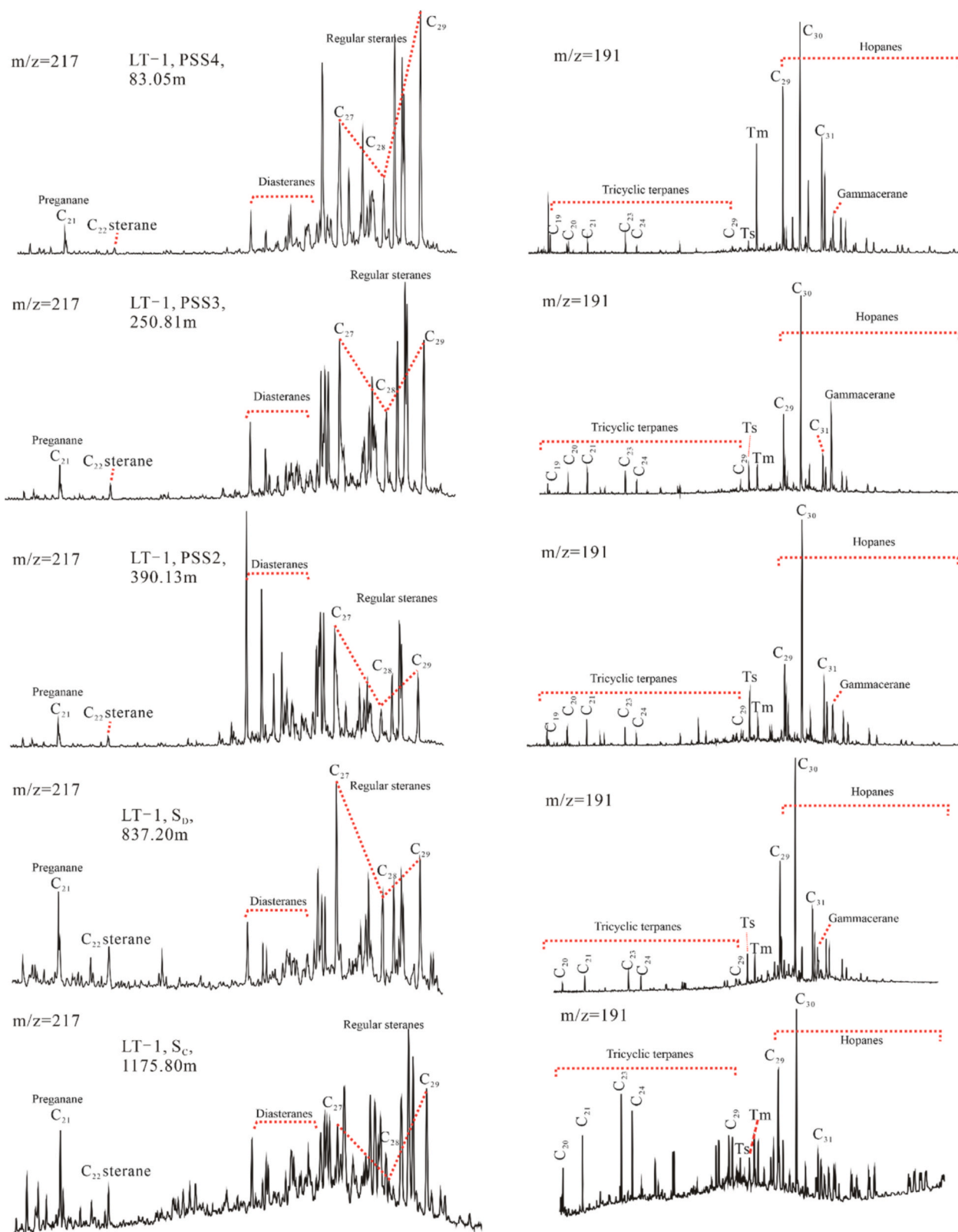


Fig. 7. Mass fragmentograms of the saturated hydrocarbon fractions with $m/z = 217$ and $m/z = 191$, for the core samples of the Xiguayuan Formation in the Luanping Basin. Ts = 18 α (H)-22, 29, 30-trinorhopane; Tm = 17 α (H)-22, 29, 30-trinorhopane.

value of 0.19 (Table 3).

It is worth noting that the terpanes (gammacerane and tricyclic terpanes) concentration of some samples below the conglomerate with a poor signal-to-noise ratio (SNR) were too low to be detected,

particularly for the samples in S_A and S_B (Fig. 7). The signals may be attributed to low concentrations of biomarker compounds, which commonly occur in high maturity source rock extracts and light oils (Peters et al., 2005). Both Huang et al. (2017) and Patra et al. (2018)

Table 3

Selected sterane and terpane parameters for K_{1x} samples in Well LT-1 from the Luanping Basin (1: C₂₇ααα(20R), %; 2: C₂₈ααα(20R), %; 3: C₂₉ααα(20R), %; 4: C₂₉ααα(20R)/C₂₇ααα(20R); 5: C₂₈ααα(20R)/C₂₇ααα(20R); 6: C₂₉ααα(20S)/(20S + 20R); 7: C₂₉αββ/(αββ+ααα); 8: Ts/Tm; 9: GI; 10: C₂₀/C₂₃ tricyclic terpane; 11: C₂₁/C₂₃ tricyclic terpane).

	Subunit	Depth, m	1	2	3	4	5	6	7	8	9	10	11
K _{1x}	PSS4	75.50	47.15	15.12	37.73	0.80	0.32	0.45	0.43	0.75	0.47	0.84	1.19
		83.05	37.49	16.17	46.34	1.24	0.43	0.46	0.39	0.10	0.08	0.86	0.79
		97.80	32.90	18.74	48.36	1.47	0.57	0.48	0.45	0.29	0.26	0.72	0.85
		110.98	47.76	22.59	29.65	0.62	0.47	0.47	0.49	0.84	0.26	0.84	1.01
		134.33	23.58	25.13	51.29	2.18	1.07	0.45	0.49	2.48	0.74	0.41	0.83
	PSS3	220.55	53.76	15.39	30.85	0.57	0.29	0.50	0.52	0.48	0.13	0.71	0.87
		250.81	38.96	22.03	39.01	1.00	0.57	0.45	0.51	0.80	0.58	0.56	0.90
	PSS2	336.00	30.92	23.42	45.66	1.48	0.76	0.44	0.54	0.82	0.78	0.53	0.85
		363.30	40.91	20.28	38.81	0.95	0.50	0.45	0.57	0.85	0.80	0.57	0.90
		378.52	46.57	20.30	33.13	0.71	0.44	0.47	0.59	1.45	0.33	0.83	0.91
		390.13	63.35	13.89	22.76	0.36	0.22	0.44	0.57	1.67	0.30	0.94	1.31
	PSS1	400.90	40.07	19.01	40.93	1.02	0.47	0.38	0.40	0.69	0.34	0.74	1.07
		472.70	40.82	23.58	35.61	0.87	0.58	0.45	0.52	0.25	0.58	1.68	0.84
S _D	773.30	34.19	30.62	35.19	1.03	0.90	0.34	0.37	0.90	0.16	0.85	0.77	
	837.20	48.72	29.38	21.90	0.45	0.60	0.55	0.55	1.01	0.17	0.62	0.83	
S _C	921.15	29.26	25.19	45.55	1.56	0.86	0.51	0.58	1.12	–	–	–	
	982.45	55.60	25.09	19.31	0.35	0.45	0.52	0.57	0.40	0.18	1.96	1.27	
	992.85	37.40	22.61	39.99	1.07	0.60	0.50	0.54	0.61	0.28	–	–	
	1016.65	40.83	23.64	35.53	0.87	0.58	0.46	0.42	0.51	–	–	–	
	1028.20	36.33	27.36	36.31	1.00	0.75	0.34	0.37	0.55	–	–	–	
S _B	1041.50	35.09	28.65	36.25	1.03	0.82	0.45	0.39	0.67	0.16	0.84	0.82	
	1124.72	28.57	13.18	58.26	2.04	0.46	0.51	0.58	0.67	–	0.50	0.75	
	1127.11	28.99	10.33	60.68	2.09	0.36	0.50	0.58	–	–	0.66	0.82	
	1136.08	34.47	10.19	55.34	1.61	0.30	0.52	0.55	–	–	1.26	1.10	
S _A	1175.8	28.50	9.56	61.94	2.17	0.34	0.50	0.54	0.72	–	0.45	0.69	
	1254.63	50.41	30.86	18.72	0.37	0.61	–	–	–	–	0.45	0.69	

noted that high thermal maturity can lead to a significant decline in terpenoid content.

4.2. Inorganic geochemical characteristics

4.2.1. Major elements

SiO₂ is the dominant major oxide in all samples, with contents ranging from 49.62 % to 63.45 % and an average value of 58.12 % (Table S1). The MnO content is the lowest, with an average of 0.09 %. Most of the major element contents, such as those of TiO₂ or P₂O₅, are relatively uniform in the samples from both above and below the conglomerate, although significant differences exist in Na₂O and K₂O contents. The K₂O content in the samples above the conglomerate (3.22%–4.08 %, 3.80 % on average) is lower than in samples below the conglomerate (3.55%–7.56 %, 5.00 % on average). The Na₂O content in the samples above the conglomerate (2.12 % on average) is lower than that in samples below the conglomerate (3.63 % on average).

4.2.2. Trace elements

The highest trace element content in the study area is that of Sr, in the range of 290.92–694.40 μg/g. Most of the trace element contents are relatively uniform, although Ni and Ba vary significantly. The Ni contents in the samples above the conglomerate (11.73–25.48 μg/g) are lower than those below the conglomerate (25.87–42.14 μg/g). The Ba contents in the samples above the conglomerate (346.16 μg/g on average) are lower than those below the conglomerate (588.26 μg/g on average). The Mo contents of samples in PSS2, PSS3, S_B and S_C are notably higher than those in adjacent subunits (Table S2).

REE contents and associated geochemical parameters for K_{1x} samples in Well LT-1 from the Luanping Basin are listed in Table S3. The total REE contents (∑REE) range from 197.02 to 680.73 μg/g, with an average of 353.32 μg/g. These values are notably higher than in the North American shale composite (NASC; 167.41 μg/g; Haskin et al., 1968), Post-Archean Average Australian Shale (PAAS; 183.03 μg/g; Taylor and McLennan, 1985), and worldwide black shales (134.19 μg/g; Ketris and Yudovich, 2009). The L/H (∑LREE/∑HREE) ratios range from 5.83 to 9.31, with an average of 7.57, and La_N/Yb_N ratios range

from 0.70 to 1.67, with an average of 1.20 (Table S3).

5. Discussion

5.1. Type and source of organic matter

Types and sources of organic matter are important for the evaluation of the hydrocarbon generation potential. They are also the factors controlling whether the products are mainly oil-prone or gas-prone (Tissot and Welte, 1984). In the cross plot of HI versus T_{max} (Fig. 8B), the organic matter types in the K_{1x} samples are mainly type II and type III, which primarily generate mixed oil and gas (dominantly oil). In the cross plot of TOC versus HI (Fig. 9B), most of the studied samples plot in the zones of fair oil and gas-oil source rocks. This implies that the K_{1x} source rocks in the Luanping Basin mainly generate oil and some gas, as also confirmed by the hydrocarbon species in Well LT-1 (Figs. 4 and 9).

Organic matter types can be identified by atomic H/C versus O/C ratios or the van Krevelen diagram (Van Krevelen, 1961; Tissot et al., 1974). As discussed above, the kerogen types identified in the Rock-Eval analysis can be generally confirmed by the kerogen atomic ratios in the H/C–O/C plot. Based on the Van Krevelen kerogen type diagram (Fig. 8A; Table 1), most K_{1x} core samples are dominated by type II kerogen. Furthermore, the O/C atomic ratios of the outcrop samples in the WJG section are higher than those of core samples, which are dominated by type II and type III kerogen (Fig. 8A).

Kerogen carbon isotopes are also used to implicate the source and type of organic matter (Huang et al., 1984; Wang et al., 1997). Compared with aquatic organisms, terrestrial plants are enriched in heavy carbon isotopes, and the heavier kerogen carbon isotope generally reflects terrestrial plant contributions. According to Fig. 8A, the δ¹³C values for the majority of the samples are heavy, suggesting an input of terrestrial plants. However, kerogen carbon isotopic composition can also be affected by precursor material and diagenetic evolution. According to the vitrinite reflectance results (Table 1; Fig. 12A), the Ro values for those samples are lower than 1.4 %. The Ro values for the WJG samples are lower than those for other core samples, while the kerogen δ¹³C values are lighter than those for core samples (Fig. 8A).

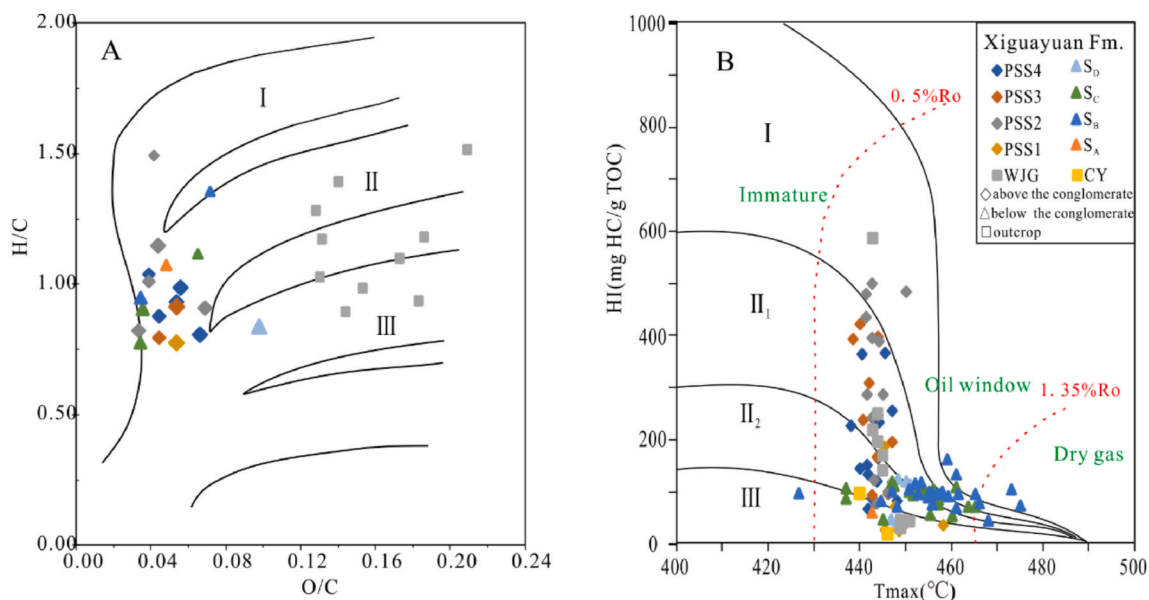


Fig. 8. (A) Van Krevelen kerogen type diagram (Hunt, 1996); (B) Cross plots of Rock-Eval S1+S2 versus TOC of the Xiguayuan Formation core samples in Well LT-1.

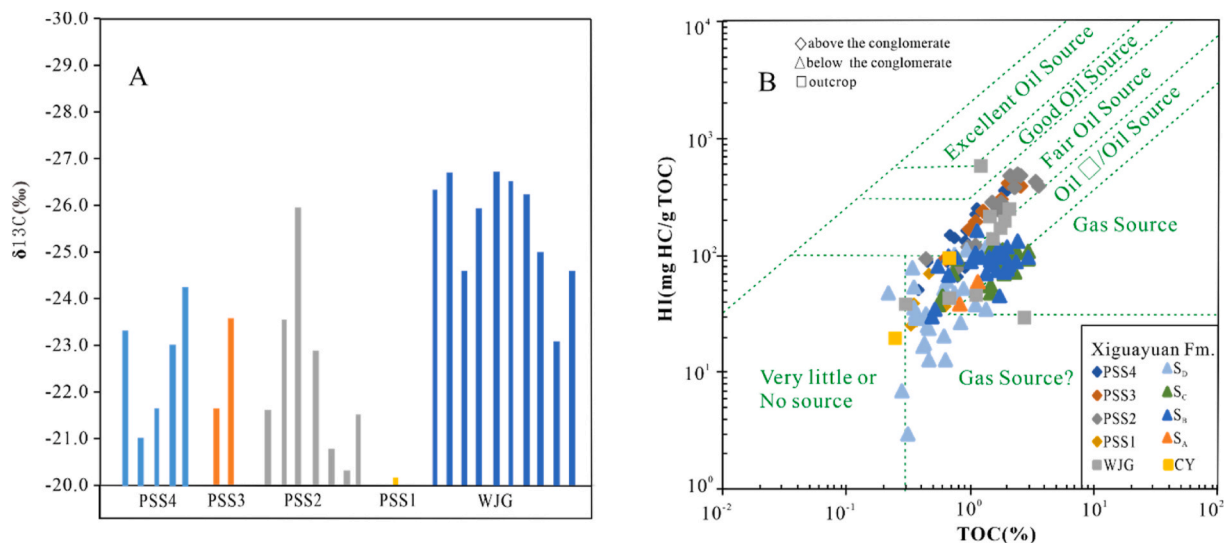


Fig. 9. (A) Histogram of kerogen carbon isotope values ($\delta^{13}\text{C}$) (modified after Huang et al., 1984; Cao et al., 2018); (B) plot of TOC versus HI for the Xiguayuan Formation core samples in Well LT-1 (modified after Tissot and Welte, 1984; Gao et al., 2017).

Xiong et al. (2004) overserved that at the stage of $R_o < 1.5\%$, the kerogen $\delta^{13}\text{C}$ values increased 3.8 % with the increasing thermal evolution.

The biomarkers characteristics are commonly used to analyse the source input and organic type of source rocks (Peters et al., 2005). According to Fig. 4 and Table 2, the n -alkane profiles of the K_{1x} samples below the conglomerate are characterised by medium-molecular-weight ($n\text{-C}_{17}\text{-}n\text{-C}_{21}$) with a weak odd-even predominance ($\text{OEP} \approx 1$), which suggests input of plankton and benthic algae. The n -alkane profiles of the source samples above the conglomerate are characterised by a weak bimodal pattern and $n\text{-C}_{23}$ predominance in n -alkanes, implying a mixed source of both terrigenous and aquatic organic matter (Eglinton and Hamilton, 1967; Scalan and Smith, 1970). As shown in Fig. 10, most samples above the conglomerate plot in the area of salty lacustrine type II kerogen, while the samples below the conglomerate show the characteristic of type II and III mixing. Organic matter of the K_{1x} was mainly derived from aquatic plankton and terrigenous higher plants.

The characteristics of regular steranes ($\text{C}_{27}\text{-C}_{29}$) could provide

abundant information on the organic source of organic matters (Peters et al., 2005; Kong et al., 2020). In particular, C_{27} and C_{29} sterols are commonly derived from algae and higher plants, respectively (Huang and Meinschein, 1979; Mashhadi and Rabbani, 2015). According to Fig. 11B and Table 3, only the PSS4 samples show the distributions of $\text{C}_{29} > \text{C}_{27} > \text{C}_{28}$, indicative of high inputs of land plants. Most samples plot in the area of plankton, algae, and bacteria with C_{27} predominance. For most samples above the conglomerate, the source of organic matter is mainly a mix of plankton and terrigenous higher plants. For most samples below the conglomerate, the source is mainly plankton and algae, but some samples show land plant inputs.

The distribution of tricyclic, especially short-chain tricyclic terpanes, can reflect sources of organic matter (Cao et al., 2018). The C_{19} and C_{20} have been interpreted to derive from terrigenous organic matter (Noble et al., 1985; Ozelik and Altunsoy, 2005), while C_{23} is thought to derive from algae (Azevedo et al., 1992). The samples above the conglomerate are characterised by the distributions of $\text{C}_{23} > \text{C}_{21} > \text{C}_{20}$ and $\text{C}_{21} > \text{C}_{23} > \text{C}_{20}$ (Fig. 6), indicative of mixed inputs between algal and terrigenous

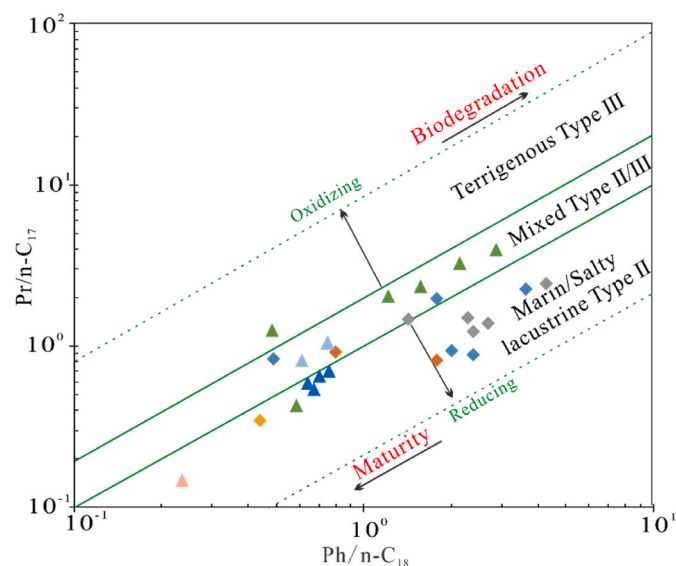


Fig. 10. (A) Plot of Pr/n-C₁₇ versus Ph/n-C₁₈ ratios of the Xiguayuan Formation core samples in Well LT-1.

plants. As for the samples below the conglomerate, most follow the order of $C_{20} > C_{23} > C_{21}$ (Fig. 6), which seems to suggest that higher land plants are the main source of organic matter. This is inconsistent with the above discussion on the source of organic matter. Theoretically, the inconsistency of biomarkers reflecting the source of organic matter, like terpanes, might be caused by complex factors, such as biodegradation, weathering, and high maturity. However, since the distribution of biomarkers does not show any characteristics of biodegradation and weathering (Fig. 5; see discussion in the *n*-alkanes section), we speculate that the high maturity is a more likely factor responsible for the absence of terpanes in these samples (Lewan et al., 1986; Peters et al., 1990, 2005).

Taking the discussion outlined above into consideration, we conclude that the organic matter in the K_{1x} mudrock is of types II and III, dominantly sourced from aquatic plankton and algae, with minor contribution of terrigenous higher plants.

5.2. Maturity of organic matter

The maturity of organic matter is an important indicator for the

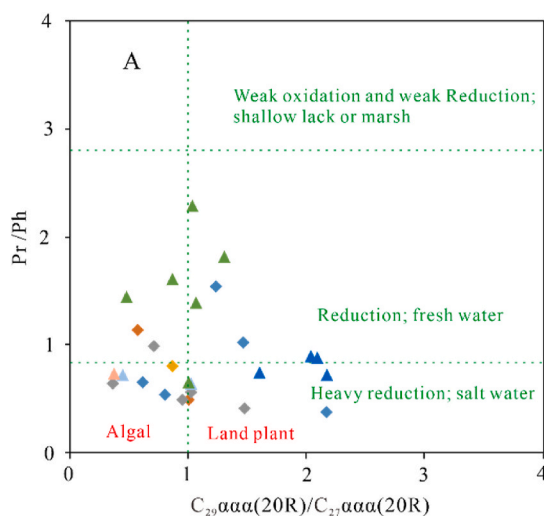


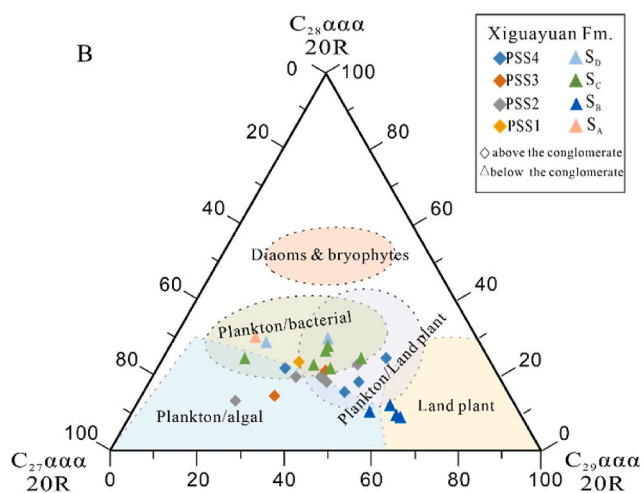
Fig. 11. (A) Plot of C₂₉ααα(20R)/C₂₇ααα(20R) sterane vs. Pr/Ph ratios; (B) Ternary plot of regular steranes C₂₇–C₂₉ showing the distribution of steranes and organic matter input in the Xiguayuan Formation core samples in Well LT-1.

evaluation of the actual hydrocarbon (oil or gas) potential of effective source rocks. Hydrocarbons (oil, wet gas, and final dry gas, pyrobitumen) were generated at different maturities (Tissot and Welte, 1984; Peters and Cassa, 1994). The Ro (vitrinite reflectance), Rock-Eval T_{max} and biomarker parameters are commonly used to evaluate the maturities of source rocks. According to Figs. 12A and B and Table 1, the maturities of the samples below the conglomerate are slightly higher than of the samples above the conglomerate. The majority of the K_{1x} samples are within the oil window and have generated a large amount of oil, which is confirmed by the presence of hydrocarbon in Well LT-1 during the drilling process (Fig. 2). The Ro values for the outcrop samples in the WJG section are distinctly lower than those for the core samples and show low maturities. It indicates that all samples from the Xiguayuan Formation (K_{1x}) show degrees of thermal evolution from moderate to high maturity.

Biomarker parameters are usually used to evaluate the thermal maturities of source rocks. The Ph/n-C₁₈ value decreases with increasing thermal maturity (Ten Haven et al., 1987), while the Ts/Tm value and the ratio of C₂₉ sterane isomerization parameters C₂₉ααα 20S/(20S + 20R) and C₂₉αββ/(αββ+ααα) have a positive relationship with thermal maturity (Seifert and Moldowan, 1986; Peters et al., 2005). It is worth noting that different biomarker parameters have different application scopes and conditions when they are applied to reflect the maturity of organic matter. According to Fig. 13 and Table 3, the ratios of C₂₉ sterane isomers of the samples above the conglomerate are lower than those of the samples below the conglomerate, which reach the equilibrium value (0.52–0.55 and 0.67–0.71 for C₂₉ααα 20S/(20S + 20R) and C₂₉αββ/(αββ+ααα), respectively) (Seifert and Moldowan, 1986). This indicates that the thermal maturities of samples below the conglomerate are higher than those of samples above the conglomerate, consistently with the Ro values. The samples below the conglomerate have relatively low Ts/Tm values and imply low thermal maturities. This is inconsistent with other maturity parameters discussed above. This inconsistency may be contributed to the difference in the sources of organic matter and the lithology of source rocks (Peters et al., 2005).

5.3. Sedimentary environment of organic matter

The distribution, composition and relative concentration of biomarkers and major elements and REE in source rocks have been efficiently analysed to indicate the sedimentary environments of organic matter, such as redox conditions, paleosalinity and paleoclimate (Didyk et al., 1987; Worash, 2002; Peters et al., 2005; Pan et al., 2020). In this



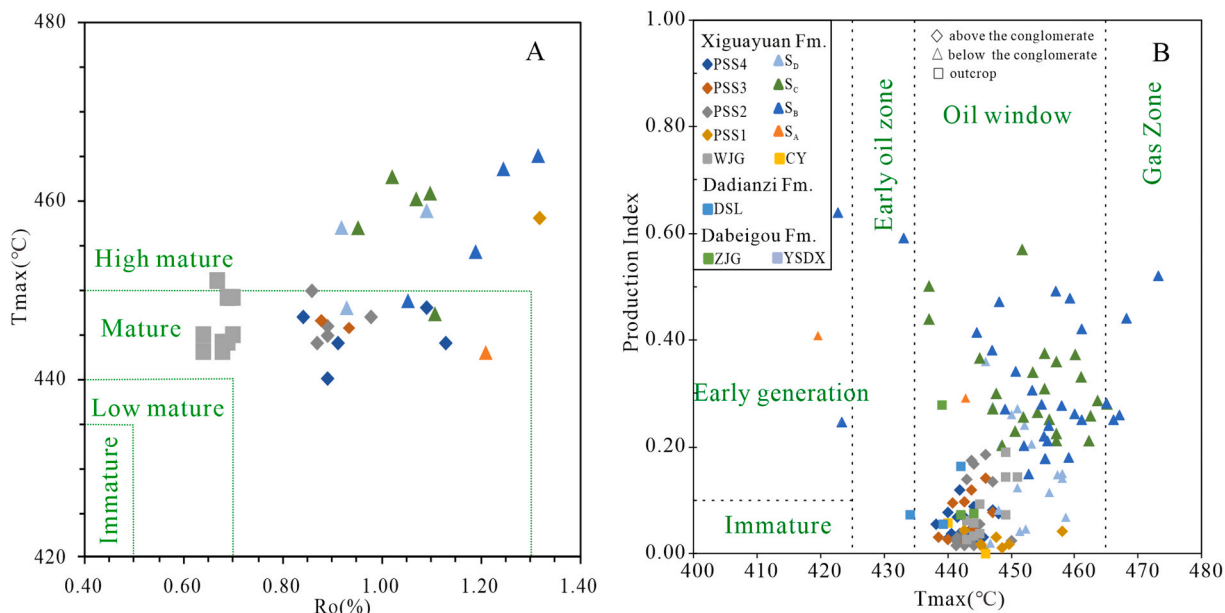


Fig. 12. (A) Cross plot of Ro (%) versus T_{max} ; (B) Cross diagram of T_{max} versus Production Index for K_1x black mudstones and shales in the Luanping Basin, (cf. Peters, 1986; Gao et al., 2017).

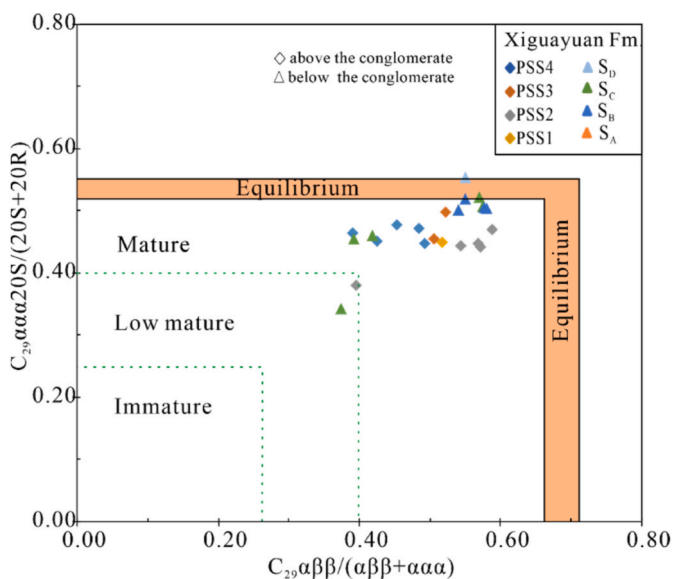


Fig. 13. Cross plot of $C_{29}\alpha\beta\beta/(\alpha\beta\beta+\alpha\alpha\alpha)$ steranes versus $C_{29}\alpha\alpha\alpha 20S/(20S + 20R)$ steranes from core samples for the Xiguayuan Formation in the Luanping Basin (cf. Seifert and Moldowan, 1986; Peters et al., 2005).

part of the study, the analysis of the K_1x source rocks is based on the core samples in Well LT-1.

5.3.1. Redox condition

The Pr/Ph values are widely used as common indicators of redox environments (Ten Haven et al., 1987; Peters et al., 2005). These values range from 0.2 to 0.8 and from 0.8 to 2.8, indicating heavy reducing and reducing environments, respectively (Mei and Liu, 1980; Li et al., 2021). According to Fig. 19 and Table 2, the Pr/Ph values for most samples above the conglomerate are less than 0.8, while those below the conglomerate are in the range of 0.8–2.8. This result indicates that the mudrocks above the conglomerate were deposited in a saline water environment under heavy reducing conditions, while the mudrocks below the conglomerate were produced in a reducing environment.

The $V/(V + Ni)$ value reflects the stratification and redox conditions. The $V/(V + Ni)$ values are in the range of 0.46–0.60 and 0.54–0.82, indicating dysoxic and anoxic conditions, respectively, where the value greater than 0.84 indicates euxinic conditions (Hatch and Leventhal, 1992). As shown in Table S2 and Figs. 14 and 17, the $V/(V + Ni)$ values range 0.72–0.85, indicating anoxic to euxinic conditions. The Mo content is enriched in euxinic environments and it could be applied to distinguish anoxic from euxinic environments (Meyer et al., 2008; Wei et al., 2021). Mo contents of 5–40 ppm indicate euxinic environments (Piper, 1994; Luo et al., 2013). The Mo contents in LT-1 vary with depth from 0.49 to 36.10 ppm (mean = 9.09 ppm), indicating euxinic environments. Furthermore, the Mo content of samples (in PSS2, PSS3, S_B and S_C) are higher than those of the adjacent subunits, which are consistent with the distribution of TOC contents.

The REE enrichment and depletion in sediments, such as Eu and Ce

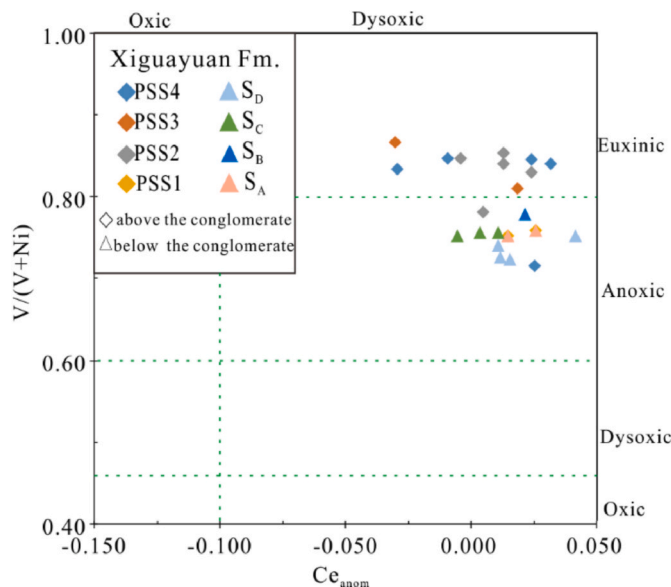


Fig. 14. Plot of Ce_{anom} versus $V/(V + Ni)$ ratios for the K_1x mudrocks in the Luanping Basin (cf. Hatch and Leventhal, 1992; Wright et al., 1987).

anomalies (δEu ; δCe ; Ce_{anom}), are commonly used to identify the sedimentary environments (Wright et al., 1987; Holser, 1997; Shields and Stille, 2001; Cao et al., 2012; Wang et al., 2015). As shown in Table S3, δEu and δCe of the K_{1x} source rocks range from 0.52 to 1.13 and from 0.92 to 1.1 respectively, demonstrating a slight Eu depletion and Ce enrichment, reflecting dysoxic deposition conditions (Holser, 1997; Shields and Stille, 2001; Cao et al., 2012). For the Ce_{anom} values of all samples greater than -0.1 , reducing dysoxic water volume environments can be implied. This is consistent with the redox values for the K_{1x} mudrocks discussed above (Wright et al., 1987, Fig. 14).

5.3.2. Paleosalinity

High GI is generally considered as an indicator of salinity and stratification of water column (Damsté et al., 1995; Hakimi et al., 2016; Li et al., 2021). According to the distribution of GI values in Well LT-1 (Table 3 and Fig. 17), the paleosalinity of the source rocks during deposition above the conglomerate in the Xiguayuan Formation is higher than that of the source rocks below the conglomerate.

The boron content in water has been demonstrated to be positively correlated with salinity. Walker and Price (1963) proposed 'adjusted boron' content formula ($B_{\text{adjusted}} = 8.5 \times B_{\text{samples}}/K_2O_{\text{samples}}$) and applied departure curve to work out equivalent boron contents (Fig. 15). Adams et al. (1965) proposed the Adams formula ($S_p = 0.0977B_E - 7.043$, where S_p represents the paleosalinity (unit in ‰) and B_E represents equivalent boron) to calculate the paleosalinity. As shown in Table S2, paleosalinity values range from 2.23 ‰ to 22.27 ‰ with an average of 9.02 ‰, reflecting brackish-saline water conditions during mudrock deposition.

During the deposition process, the adsorption capacity of clay minerals for K and Na increases with increasing water salinity, and the adsorption amount of K is larger than Na. The higher the salinity, the larger the K/Na ratio of the sediment (Jiao et al., 2004). The Sr/Ba ratio is usually applied to reflect paleosalinity of the water column and paleoclimate (Deng and Qian, 1993; Gang and Zhou, 2007; Xi et al., 2011). In lacustrine environments without marine transgression, a Sr/Ba ratio of 0.5–1.0 usually indicates brackish water environments in

semiarid to semi-moist climates, while values > 1.0 indicate high-salinity and arid environments (Shi et al., 2003; Wang et al., 2015). As shown in Fig. 16A and Table S2, the Sr/Ba ratios for the samples above the conglomerate (PSS1–PSS4), with an average value of 2.06, indicate high-salinity. Conversely, the samples below the conglomerate (S_A – S_D), have Sr/Ba ratios of 0.72 on average, implying a brackish water environment, which is consistent with the trend of K/Na ratio values and GI (Fig. 16A and B). To summarise, these sedimentary parameters (biomarkers and inorganic elements) reflect a brackish high-salinity water sedimentary environment.

5.3.3. Paleoclimate

For a lake, paleoclimate has a controlling effect on the paleo-productivity, redox conditions of sedimentary water column and supply of terrigenous material. For example, the migration and distribution of humid (Fe, Mn, Cr, V, Co, and Ni) and arid (Ca, Mg, K, Na, Sr and Ba) climatic elements are closely related to paleoclimate. Many scholars successfully used the C-value ($\Sigma(\text{Fe} + \text{Mn} + \text{Cr} + \text{Ni} + \text{V} + \text{Co})/\Sigma(\text{Ca} + \text{Mg} + \text{Sr} + \text{Ba} + \text{K} + \text{Na})$) to study paleoclimate (Zhao et al., 2007; Cao et al., 2012; Wang et al., 2015). In a continental basin, high Sr concentrations are generally related to evaporation of lake water in arid and hot climates. Liu et al. (2007) proposed that the Sr/Cu ratio in the range of 1–10 indicates a warm and moist climate, while that greater than 10 indicates a hot and arid climate. For the studied samples, the C-value and Sr/Cu ratio show an overall negative correlation (Fig. 17A), indicating a semiarid climate condition (Fig. 17A, and Tables S1 and S2).

The distribution of major elements (SiO_2 , Al_2O_3 , K_2O and Na_2O) can be used to constrain the paleoclimate during sediment deposition (Suttner and Dutta, 1986; Adegoke et al., 2014). According to Fig. 17B, the K_{1x} samples consistently plot in the area of the semiarid climate. This is consistent with the above discussion of C-values and Sr/Ba ratios, and with the brackish high-salinity water environments (Tables S1 and S2).

5.3.4. Paleoproductivity

Phosphorus (P) is an important nutrient element of plankton, and it is regarded as a vital factor in controlling paleoproductivity (Holland, 1978; Schoepfer et al., 2015; Wei et al., 2021). The P/Ti ratio is commonly used as an indicator of paleoproductivity to characterise the nutritional status of ancient lakes (Algeo et al., 2011). According to Table S2 and Fig. 19, P/Ti ratios of all studied samples range from 0.26 to 0.77 with an average of 0.47, which are between moderate (Ubara section, the average P/Ti ratio of the chert is 0.34) and high (Ubara section, the average P/Ti ratio of black shale is 0.79) productivity. It indicates a moderate paleoproductivity during their deposition, related to semiarid paleoclimate. The K_{1x} mudrocks are enriched in P with an average value of 0.33 ‰, which is notably higher than that of average shale (0.19 ‰) and NASC (0.13 ‰). Moreover, in PSS2, PSS3, S_C and S_B subunits, the P/Ti ratios for the samples are higher than those for the adjacent subunits, varying in similar ranges as the TOC.

Because of the volcano eruption in Luanping Basin, multiple tuff intervals and volcanic ash layers were commonly observed in Well LT-1 (Figs. 18 and 19). The input of volcanic ash is indicated by a tuffaceous composition of the interbedded mudstone and carbonate layers (Tao et al., 2013, Fig. 18). Sufficient nutrients (such as P, N and Fe) can be provided by volcanic ash for the development of algae and plankton, forming reducing sedimentary environments conducive for the preservation of organic matter (Hamme et al., 2010; Langmann et al., 2010; Tao et al., 2013).

5.3.5. Sedimentary rate

The mudstone sedimentary rate could be obtained by the fractionation of REEs, which can be assessed by the La_N/Yb_N ratio (ratio of La to Yb, normalised to the NASC). The closer the value is to 1, the weaker is the REE fractionation and the faster is the sedimentary rate (Tenger et al., 2006; Wang et al., 2015; Chen et al., 2019). As shown in Table S3

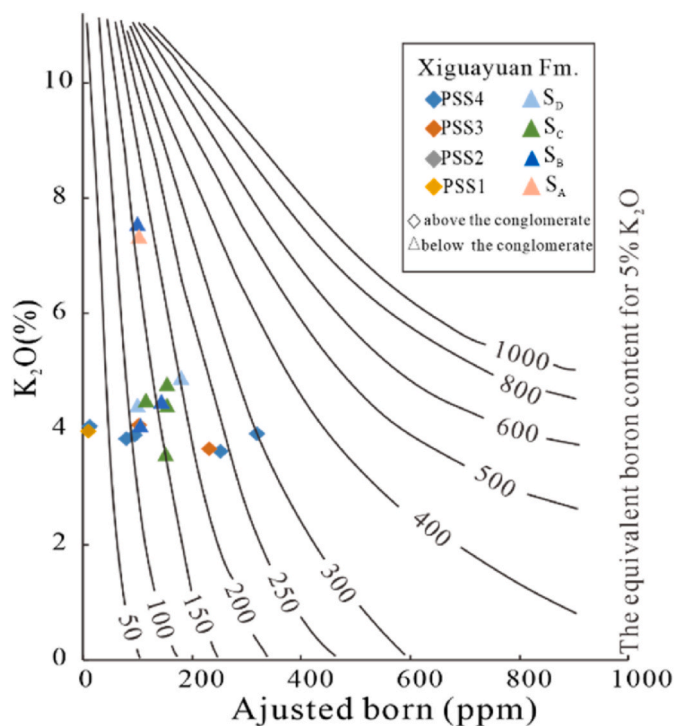


Fig. 15. Departure curves for the calculation of equivalent boron (Walker and Price, 1963).

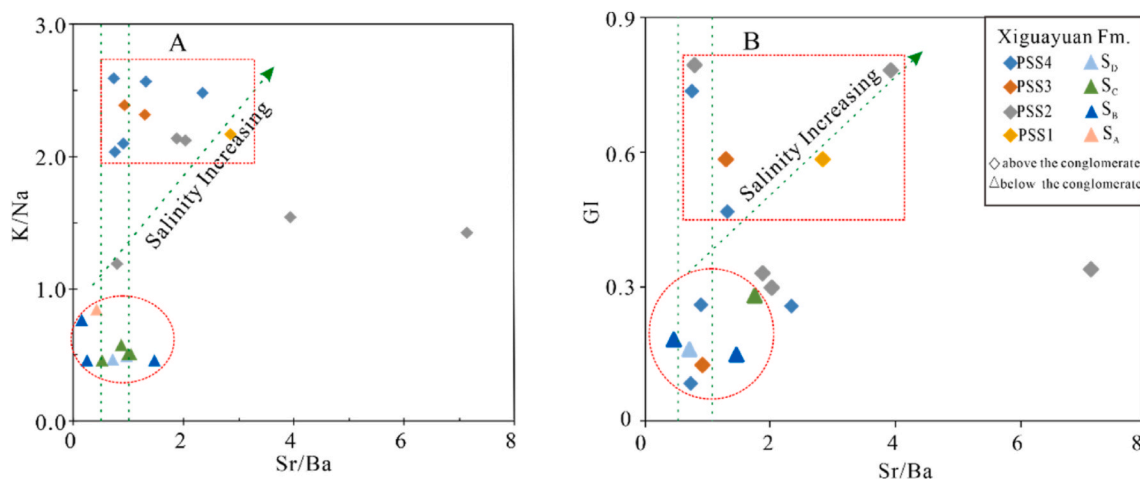


Fig. 16. (A) Plot of Sr/Ba versus K/Na ratios; (B) Plot of Sr/Ba ratio versus GI for the K_1x mudrocks in the Luanping Basin.

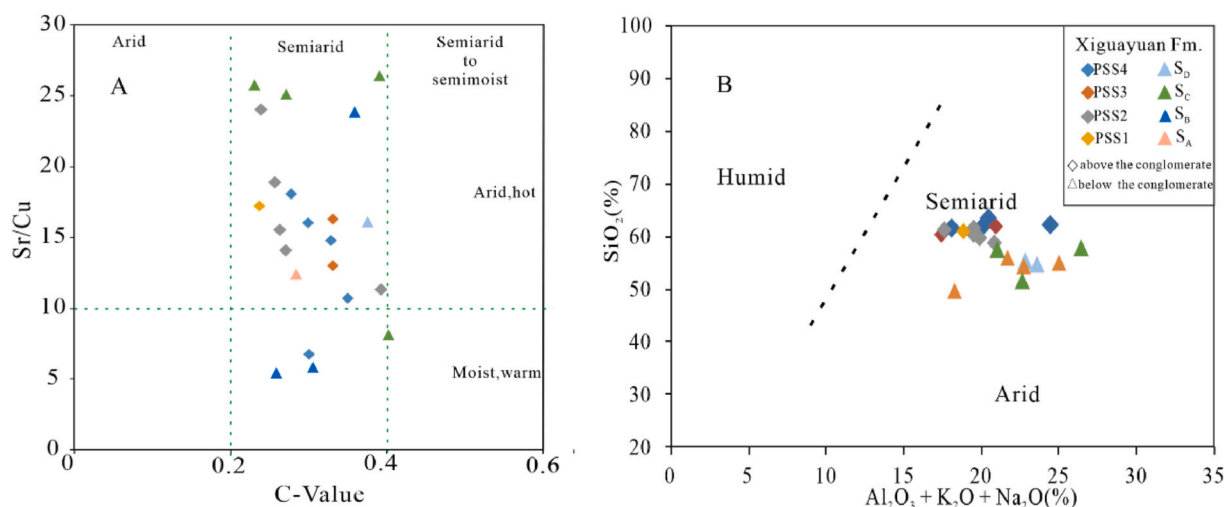


Fig. 17. (A) Plot of C-value versus Sr/Cu ratios; (B) a binary ($Al_2O_3 + K_2O + Na_2O$) versus SiO_2 diagram for the K_1x black mudrocks in the Luanping Basin (cf. Suttner and Dutta, 1986).

and Fig. 19, the $(La/Yb)_N$ ratio values for the samples above the conglomerate vary from 0.98 to 1.25 (mean = 1.15), while those for the samples below the conglomerate vary from 0.70 to 1.67 (mean = 1.26). This indicates generally fast-sedimentary rates during mudrock deposition, with faster sedimentary rates for the mudrock above the conglomerate.

Based on the zircon U–Pb dating of two 520-m-separated tuff samples at the bottom of Well LT-1, their ages are 127.6 Ma and 123.31 Ma, respectively (Fig. 19). Shen et al. (2015) proposed that linear sedimentary rates (LSRs) could be used to calculate sedimentation rates and fluxes for the stratigraphic interval of interest. LSRs were calculated as $LSR = \text{thickness}/\text{duration}$, resulting in 121.21 mMa^{-1} , which reflects a fast-sedimentary rate.

5.3.6. Organic matter accumulation and sedimentary environment

The accumulation of organic matter is influenced by many factors, including: (1) paleoproductivity (input); (2) preservation (redox and paleosalinity); and (3) sedimentary rate (dilution or exposure oxidation) (Wang et al., 2015). The exchange of nutrients and oxygen above and below the chemocline can be hindered by the vertical salinity stratification of lake water bodies. It is conducive to form an anoxic environment for the development of high-quality source rocks (Wei et al., 2021). The accumulation of organic matter can be affected by factors such as

input, preservation, and dilution of organic matter (Talbot, 1988; Pedersen and Calvert, 1990; Tyson, 2005). The present discussion shows that many parameters have a similar variation tendency with TOC contents in Well LT-1, such as the redox proxy Mo or the productivity P/Ti ratio proxy (Fig. 19). In PSS2, PSS3, S_C , and S_B , the TOC contents are higher than those in the adjacent subunits, reflecting good to excellent source rocks. However, the Sr/Ba, GI, and K/Na indices for the samples in the upper subunits are higher than those for the lower subunits, showing a trend different from the TOC contents (Fig. 19). This inconsistency may indicate that appropriate salinity is beneficial to the preservation of organic matter and excessive salinity is not conducive to the accumulation of organic matter.

The sedimentary environment mainly featured anoxic and brackish-saline water conditions, and the climate during organic matter deposition in the Xiguayuan Formation was semiarid. During the early stages of the Xiguayuan Formation, frequent and transient volcanic eruptions occurred in the Luanping Basin. Some nutrient elements such as P, N, and Fe were delivered by volcanic ash and terrigenous debris (Fig. 19). Nutrient elements can be released by volcanic ash, which can promote planktonic algae prosperity and improve paleoproductivity (Langmann et al., 2010; Du et al., 2020). This indicates that paleoproductivity can significantly affect the enrichment of organic matter in the mudrocks of the Xiguayuan Formation. At the same time, in the semiarid climate,

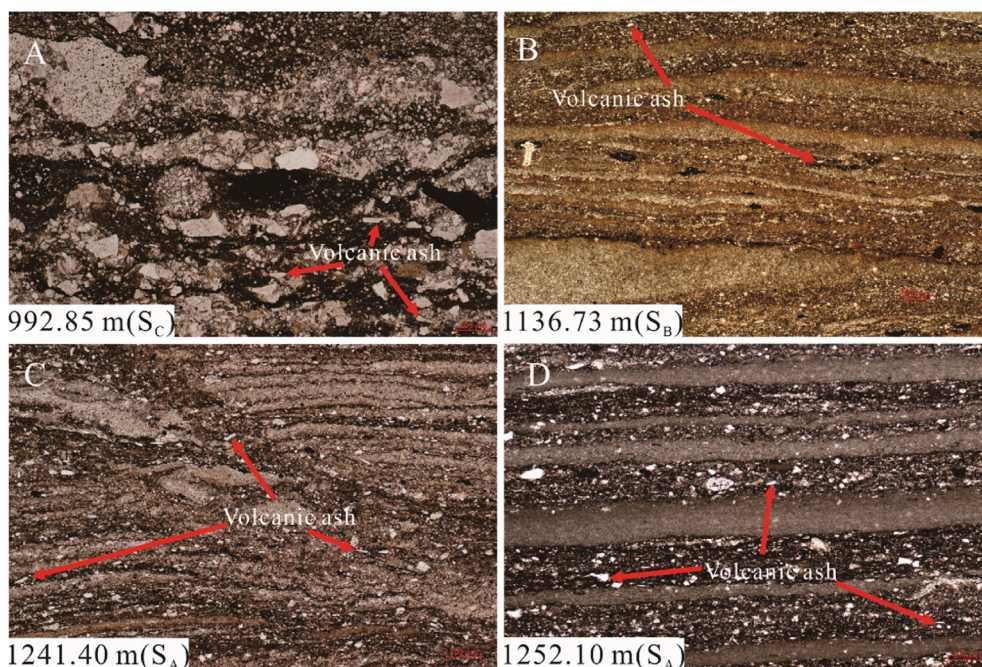


Fig. 18. The petrographic thin section photography (polarised light) of volcanic ash in mudrocks in Well LT-1.

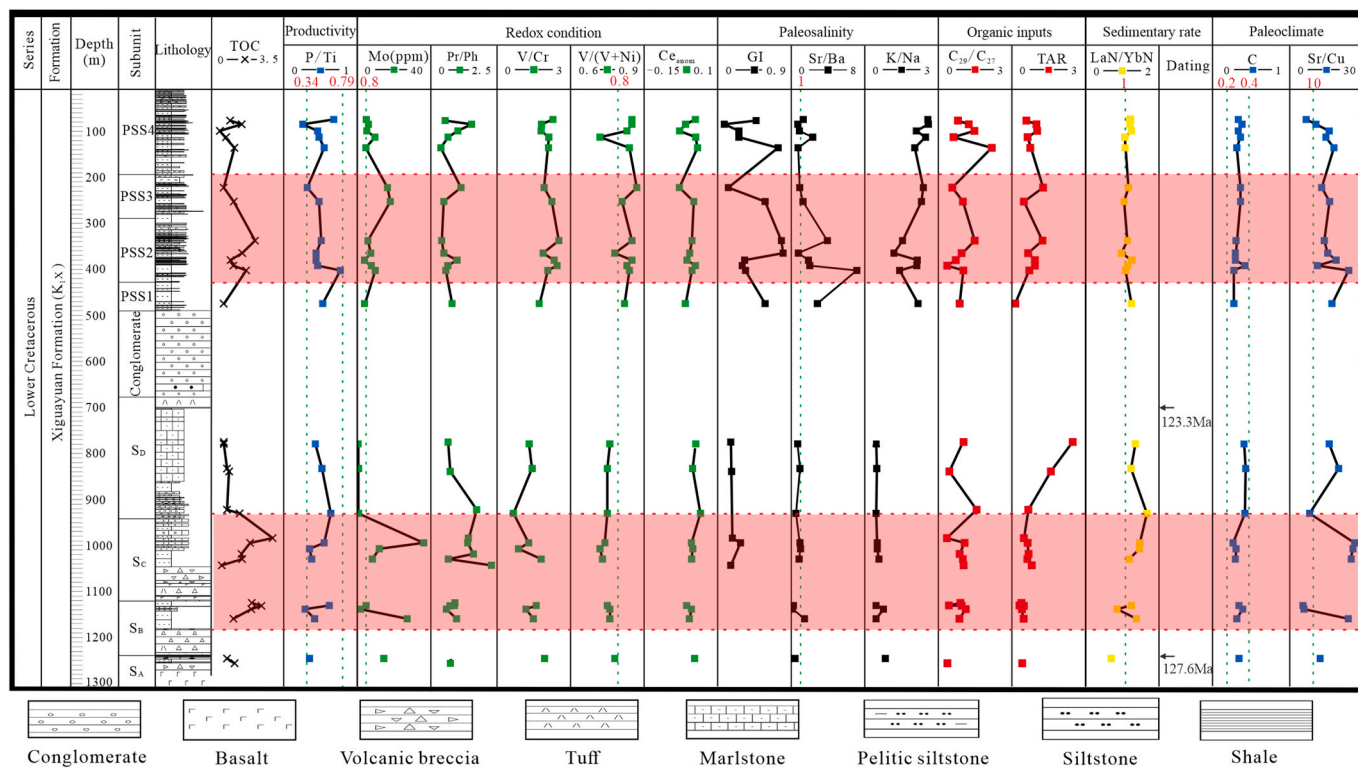


Fig. 19. Vertical variation of TOC, paleoproductivity, redox, paleosalinity, climate, sedimentary rate, and organic matter inputs in Well LT-1.

both precipitation and input of terrigenous organic matter through surface runoff are reduced, while aquatic organic matter is significantly enhanced (Fig. 20). The salinity of lake water increased with the increasing evaporation and led to the sedimentary environments of brackish water. Moreover, algae and archaea are the crucial source of organic matter in brackish to high-salinity lakes (Zhang et al., 1985; Hackley and SanFilippo, 2016). In addition to contribution of higher plants, plankton and algae inputs are significant in the lower four

subunits. Therefore, the organic matter in the K1x source rocks has likely been contributed from multiple sources. It is worth noting that the dilution effect of organic matter could be due to extremely fast sedimentary rate, which would lower the TOC content. A weaker REEs fractionation has been observed for all K1x samples, which indicates fast depositional rates when combined with the ages of the volcanic ash layers. This is one of the reasons why the TOC content is not so high in the studied samples. In summary, it can be concluded that the

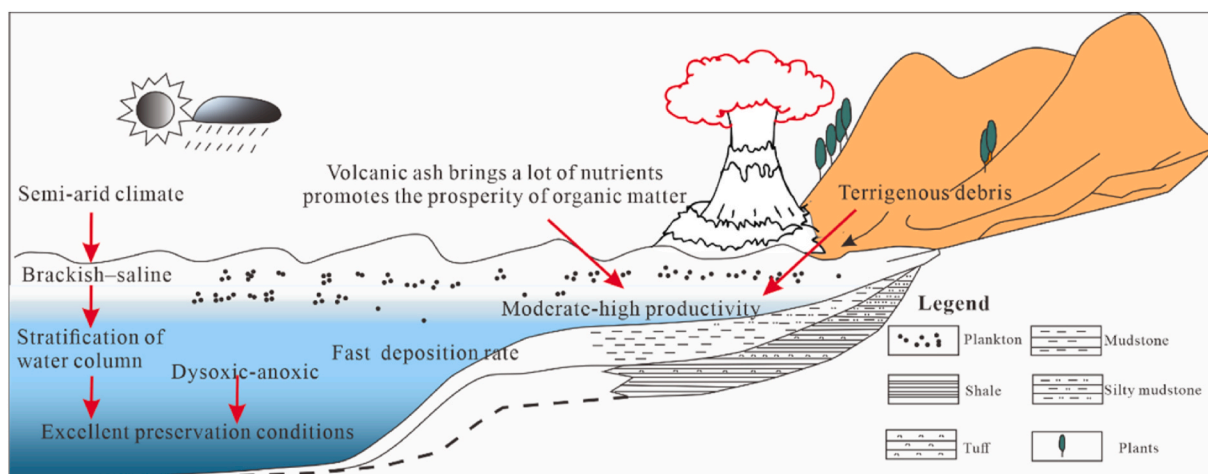


Fig. 20. Model of organic matter enrichment in the source rocks of the Xiguayuan Formation in the Luanping Basin.

hydrolysis of volcanic ash and the nutrients carried by terrigenous debris promote the paleoproductivity of organic matter. Good preservation conditions play an important role in promoting the enrichment of organic matter in source rocks, such as the redox and salinity conditions, while an extremely fast deposition rate has lowered the final TOC content (Fig. 20).

6. Conclusion

Detailed investigations of organic and elemental geochemical characteristics have been carried out on the lower Cretaceous source rocks in the Luanping Basin of the Yanshanian Structural Belt, to discuss hydrocarbon potential and sedimentary environments. The conclusions can be drawn as follows:

- (1) The four subunits (PSS2, PSS3, S_B and S_C) are the major source rock intervals of good to excellent potential in the Xiguayuan Formation. The residual source rocks only reach poor to fair standard. The kerogens of the source rocks are dominated by types II and III. The source rocks have been supplied by multiple contributions of organic matter, such as higher plants, plankton and algae. All samples are in mature to highly mature stage of thermal maturity.
- (2) In general, the K₁x mudrocks are deposited under dysoxic to anoxic lacustrine environments, and the paleosalinity of the lake water was brackish to highly saline. The paleoclimate index indicates a semiarid climate. Sufficient nutrients are brought by volcanic ash and terrigenous debris, promoting the paleoproductivity.
- (3) The high-quality source rocks have strong reducibility and higher salinity under a high productivity, such as PSS2, PSS3, S_B and S_C four subunits. Excellent preservation may be the major controlling factor of the accumulation of organic matter for the K₁x source rocks, but sedimentary rates and paleoproductivity cannot be neglected.

Declaration of competing interest

The authors declare that they have no known competing financial interests or personal relationships that could have appeared to influence the work reported in this paper.

Acknowledgement

This study was funded by the National Major Research Program for Science and Technology of China (Grant No. 2017ZX05009-002) and the

National Natural Science Foundation of China (Grant No. 41772090). The authors are also grateful to the Petroleum Geology Laboratory, China University of Petroleum (Beijing) for providing the laboratory instruments.

Appendix A. Supplementary data

Supplementary data to this article can be found online at <https://doi.org/10.1016/j.marpetgeo.2021.105256>.

References

- Adegoke, A.K., Abdullah, W.H., Hakimi, M.H., Sarki Yandoka, B.M., 2014. Geochemical characterisation of Fika formation in the Chad (Bornu) Basin, northeastern Nigeria: implications for depositional environment and tectonic Subunitting. *Appl. Geochem.* 3, 1–12.
- Algeo, T.J., Kuwahara, K., Sano, H., Bates, S., Lyons, T., Elswick, E., Maynard, J.B., 2011. Spatial variation in sediment fluxes, redox conditions, and productivity in the Permian-Triassic Panthalassic Ocean. *Palaeogeogr. Palaeoclimatol.* 308, 65–83.
- Azevedo, D.A., Neto, F.R.A., Simoneit, A.C., Pinto, B.R.T., 1992. Novel series of tricyclic aromatic terpanes characterized in Tasmanian tasmantite. *Org. Geochem.* 18 (1), 9–16.
- Bourbonniere, R.A., Meyers, P.A., 1996. Sedimentary geolipid records of historical changes in the watersheds and productivities of Lakes Ontario and Erie. *Limnol. Oceanography* 41, 352–359.
- Bray, E.E., Evans, E.D., 1961. Distribution of n-paraffins as a clue to recognition of source beds. *Geochem. Cosmochim. Acta* 22, 2–15.
- Cao, J., Wu, M., Chen, Y., Hu, K., Bian, L.Z., Wang, L.G., Zhang, Y., 2012. Trace and rare earth element geochemistry of Jurassic mudstones in the northern Qaidam Basin, northwest China. *Chem. Erde-Geochem* 72, 245–252.
- Cao, J., Yang, R., Hu, G., et al., 2018. Hydrocarbon potential of the Lower Cretaceous mudstones in coastal southeastern China. *AAPG Bull.* 102 (2), 333–366.
- Chen, Y., Zhu, Z., Zhang, L., 2019. Control actions of sedimentary environment and sedimentation rates on lacustrine oil shale distribution, an example of the oil shale in the Upper Triassic Yanchang Formation, southeastern Ordos Basin (NW China). *Mar. Petrol. Geol.* 102, 508–520.
- Cope, T., Luo, P., Zhang, X.Y., Zhang, X.J., Song, J.M., Zhou, G., Shultz, M.R., 2010. Structural controls on facies distribution in a small half-graben basin: Luanping Basin, Northeast China. *Basin Res.* 22, 33–44.
- Damsté, J.S.S., Kenig, F., Koopmans, M.P., Köster, J., Schouten, S., Hayes, J.M., de Leeuw, J.W., 1995. Evidence for gammacerane as an indicator of water column stratification. *Geochem. Cosmochim. Acta* 59, 1895–1900.
- Deng, H.W., Qian, K., 1993. *Analysis on Sedimentary Geochemistry and Environment*. Science Technology Press, Gansu, pp. 15–85 (in Chinese).
- Didyk, B.M., Simoneit, B.R.T., Brassell, S.C., Eglinton, G., 1978. Organic geochemical indicators of palaeoenvironmental conditions of sedimentation: *Nature* 272, 216–222.
- Ding, X., Liu, G., Zha, M., Gao, C., Huang, Z., Qu, J., Lu, X., Wang, P., Chen, Z., 2016. Geochemical characterization and depositional environment of source rocks of small fault basin in Erlan Basin, northern China. *Mar. Petrol. Geol.* 69, 231–240.
- Du, X., Lu, Y., Duan, D., Liu, Z., Zhao, K., Jia, J., Fu, H., 2020. Was volcanic activity during the Ordovician-Silurian transition in South China part of a global phenomenon? Constraints from zircon U–Pb dating of volcanic ash beds in black shales. *Mar. Petrol. Geol.* 114, 104209.
- Eglinton, G., Hamilton, R.J., 1967. Leaf epicuticular waxes: *Science* 1322–1335, v. 156.

- Gang, L., Zhou, D., 2007. Application of microelements analysis in identifying sedimentary environment-taking Qianjiang formation in the Jiangnan Basin as an example. *Petroleum geology and experiment* 29, 307–311 (in Chinese with English abstract).
- Gao, G., Titi, A., Yang, S., et al., 2017. Geochemistry and depositional environment of fresh lacustrine source rock: a case study from the Triassic Baijiantan Formation shales in Junggar Basin, northwest China[J]. *Org. Geochem.* 113, 75–89.
- Gao, G., Yang, S., Ren, J., Zhang, W., Xiang, B.L., 2018. Geochemistry and depositional conditions of the carbonate-bearing lacustrine source rocks: a case study from the Early Permian Fengcheng Formation of Well FN7 in the northwestern Junggar Basin. *J. Petrol. Sci. Eng.* 162, 407–418.
- Hackley, P.C., SanFilippo, J.R., 2016. Organic petrology and geochemistry of Eocene Suzak bituminous marl, north-central Afghanistan: depositional environment and source rock potential. *Mar. Petrol. Geol.* 73, 572–589.
- Hakimi, M.H., Abdullah, W.H., Al-Sharabi, M.S., Al-Samawy, H.F., Al-Borihee, K.M., Al-Qahtani, M.H., Makeen, Y.M., 2015. Indication origin and type of organic matter and its relation to depositional conditions using molecular composition and geochemical elements: the Jurassic Amran sediments from Samea area in the Taiz Governorate, Southwestern Yemen. *Arab. J. Geosci.* 8, 10151–10167.
- Hakimi, M.H., Abdullah, W.H., Alqudah, M., Makeen, Y.M., Mustapha, K.A., 2016. Organic geochemical and petrographic characteristics of the oil shales in the Lajjun area, Central Jordan: origin of organic matter input and preservation conditions. *Fuel* 181, 34–45.
- Hamme, R.C., Webley, P.W., Crawford, W.R., Whitney, F.A., DeGrandpre, M.D., Emerson, S.R., Eriksen, C.C., Giesbrecht, K.E., Gower, J.F.R., Kavanaugh, M.T., Pena, M.A., Sabine, C.L., Batten, S.D., Coogan, L.A., Grundle, D.S., Lockwood, D., 2010. Volcanic ash fuels anomalous plankton bloom in subarctic northeast. *Pacific Geophys. Res. Lett.* 37, 470–479.
- Haskin, L.A., Haskin, M.A., Frey, F.A., Wilderman, T.R., 1968. Relative and Absolute Terrestrial Abundances of the Rare Earths. In: Ahrens, L.H. (Ed.), *Origin and Distribution of the Elements*. Pergamon, Oxford, pp. 889–912.
- Hatch, J.R., Leventhal, J.S., 1992. Relationship between inferred redox potential of the depositional environment and geochemistry of the upper pennsylvanian (missourian) Stark shale member of the dennis limestone, wabaunsee county, Kansas, USA. *Chem. Geol.* 99, 65–82.
- Holland, H.D., 1978. *The Chemistry of the Atmosphere and the Oceans*. Wiley-Interscience, New York.
- Holser, W.T., 1997. Evaluation of the application of rare-earth elements to paleoceanography. *Palaeogeogr. Palaeoclimatol. Palaeoecol.* 132, 309–323.
- Huang, D.F., Li, J.C., Zhang, D.J., 1984. Kerogen types and study on effectiveness, limitation, and interrelation of their identification parameters. *Acta Sedimentol. Sin.* 2 (3), 18–33 (in Chinese with English abstract).
- Huang, H., Zhang, S., Gu, Y., Su, J., 2017. Impacts of source input and secondary alteration on the extended tricyclic terpane ratio: a case study from Palaeozoic sourced oils and condensates in the Tarim Basin, NW China. *Org. Geochem.* 112, 158–169.
- Huang, W.Y., Meinschein, W.G., 1979. Sterols as ecological indicators. *Geochem. Cosmochim. Acta* 43, 739–745.
- Hunt, J.M., 1996. *Petroleum Geochemistry and Geology*, second ed. W. H. Freeman, San Francisco, p. 743.
- Jia, H., Ji, H., Yu, J., Meng, X., 2020. Sediment supply control on the delivery of sediments to deep-lacustrine environment: a case study from Luanping Basin, northern China. *Geol. J.* 55, 3679–3693.
- Jiao, Y.Q., Wu, F.D., Li, S.T., Zhang, W.H., 2000. Diagenism and thermal fluid episode migration events in Luanping basin, China. *Acta Petrol. Sin.* 16, 615–622 (in Chinese with English abstract).
- Jiao, Y.Q., Lu, X.B., Wang, Z.H., 2004. Two distinct geological environments from sedimentary to diagenesis stages: examples from sandstone-type uranium deposits, Turpan-Hami Basin. *Earth Sci. J. China Univ. Geosci.* 29, 615–620 (in Chinese with English abstract).
- Ketris, M.P., Yudovich, Y.E., 2009. Estimations of Clarkes for carbonaceous biolithes: world average for trace element contents in black shales and coals. *Int. J. Coal Geol.* 78, 135–148.
- Kong, X., Jiang, Z., Zheng, Y., Xiao, M., Chen, C., Yuan, H., Chen, F., Wu, S., Zhang, J., Han, C., Liu, S., 2020. Organic geochemical characteristics and organic matter enrichment of mudstones in an Eocene saline lake, Qianjiang Depression, Hubei Province, China. *Mar. Petrol. Geol.* 114, 104194.
- Langmann, B., Zaksek, K., Hort, M., Duggen, S., 2010. Volcanic ash as fertiliser for the surface ocean. *Atmos. Chem. Phys.* 10, 3891–3899.
- Lewan, M.D., Bjørøy, M., Dolcater, D.L., 1986. Effects of thermal maturation on steroid hydrocarbons as determined by hydrous pyrolysis of Phosphoria Retort Shale. *Geochem. Cosmochim. Acta* 50, 1977–1987.
- Li, Q., Xu, S., Hao, F., Shu, Z., Chen, F., Lu, Y., Wu, S., Zhang, L., 2021. Geochemical characteristics and organic matter accumulation of argillaceous dolomite in a saline lacustrine basin: a case study from the paleogene xingouzi formation, Jiangnan Basin, China. *Mar. Petrol. Geol.* 128, 105041.
- Li, H., Song, Z., Zou, Y., Wang, C., Ji, Q., 2008. Characteristics of sedimentary organic matter and paleoclimate and environmental evolution during early Cretaceous time in northern part of Hebei and western of Liaoning province. *Acta Geol. Sin.-Eng* 82, 72–76.
- Liu, S., Zhang, J., Hong, S., Ritts, B.D., 2007. Early mesozoic basin development and its response to thrusting in the yanshan fold-and-thrust belt, China. *Int. Geol. Rev.* 49, 1025–1049.
- Li, Y., 2003. Fan – deltaic depositional systems of the Xiguayuan Formation in Luanping Basin. *Acta Geol. Sin.* 24, 353–356 (in Chinese with English abstract).
- Liu, Y., Tian, S., Li, P., Pang, Q., Li, Y., 2001. The stratigraphic framework of the Dabeigou-Dadianzi Formations in Luanping basin, northern Hebei and its stratotype significance. *Acta Geosci. Sin.* 22, 391–396 (in Chinese with English abstract).
- Luo, Q., Zhong, N., Zhu, L., Wang, Y., Qin, J., Qi, L., Ma, Y., 2013. Correlation of burial organic carbon and paleoproductivity in the Mesoproterozoic Hongshuihuang Formation, northern North China. *Chin. Sci. Bull.* 58, 1299–1309.
- Mashhadi, S., Rabbani, A.R., 2015. Organic geochemistry of crude oils and Cretaceous source rocks in the Iranian sector of the Persian Gulf: an oil–oil and oil–source rock correlation study. *Int. J. Coal Geol.* 146, 118–144.
- Mei, B., Liu, X., 1980. The distribution of isoprenoid alkanes in China’s crude oil and its relation with the geologic environment. *Oil Gas Geol.* 1, 99–115 (in Chinese with English abstract).
- Meyer, E.E., Burgreen, B.N., Lackey, H., Landis, J.D., Quicksall, A.N., Bostick, B.C., 2008. Evidence for basin restriction during syn-collisional basin formation in the silurian arisaig group, nova scotia. *Chem. Geol.* 256, 1–11.
- Noble, R.A., Alexander, R., Kagi, R.I., Knox, J., 1985. Tetracyclic diterpenoid hydrocarbons in some Australian coals, sediments and crude oils. *Geochem. Cosmochim. Acta* 49, 2141–2147.
- Ozcelik, O., Altunsoy, M., 2005. Organic geochemical characteristics of miocene bituminous units in the beypazari basin, central anatolia, Turkey. *Arabian J. Sci. Eng.* 30, 181–194.
- Pan, X., Wang, Z., Li, Q., Gao, J., Zhu, L., Liu, W., 2020. Sedimentary environment and mechanism of organic matter enrichment of dark shales with low TOC in the Mesoproterozoic Cuizhuang Formation of the Ordos Basin: evidence from petrology, organic geochemistry, and major and trace elements. *Mar. Petrol. Geol.* 122, 104695.
- Patra, S., Dirghangi, S.S., Rudra, A., Dutta, S., Ghosh, S., Varma, A.K., Shome, D., Kalpana, M.S., 2018. Effects of thermal maturity on biomarker distributions in gondwana coals from the satpura and damodar valley basins, India. *Int. J. Coal Geol.* 196, 63–81.
- Pedersen, T.F., Calvert, S.E., 1990. Anoxia vs. productivity: what controls the formation of organic-carbon-rich sediments and sedimentary rocks? *AAPG Bull.* 74, 454–466.
- Peters, K.E., 1986. Guidelines for evaluating petroleum source using programmed pyrolysis. *Am. Assoc. Petrol. Geol. Bull.* 70, 318–329.
- Peters, K.E., Moldowan, J.M., Sundaraman, P., 1990. Effects of hydrous pyrolysis on biomarker thermal maturity parameters: monterey phosphatic and siliceous members. *Org. Geochem.* 15, 249–265.
- Peters, K.E., Cassa, M.R., 1994. *Applied source rock geochemistry: chapter 5: Part II. Essential Elements*.
- Peters, K.E., Walters, C.C., Moldowan, J.M., 2005. *The biomarker guide. Biomarkers and Isotopes in Petroleum Systems and Earth History (Part II)*. University Press, Cambridge.
- Piper, D.Z., 1994. Seawater as the source of minor elements in black shales, phosphorites and other sedimentary rocks. *Chem. Geol.* 114, 95–114.
- Qin, Z.H., Xi, D.P., Xu, Y.K., Wei, F., Ding, C., Yu, Z.Q., Wan, X.Q., 2017. Lithostratigraphy, biostratigraphy and its geological time of the Dabeigou Formation from the yushuxia section in the Luanping Basin, northern Hebei. *Earth Sci. Front.* 24, 78–105.
- Ren, J., Tamaki, K., Li, S., Zhang, J., 2002. Late Mesozoic and Cenozoic rifting and its dynamic Subuniting in eastern China and adjacent areas. *Tectonophysics* 344, 175–205.
- Scalan, E.S., Smith, J.E., 1970. An improved measure of the odd-even predominance in the normal alkanes of sediment extracts and petroleum. *Geochem. Cosmochim. Acta* 34, 611–620.
- Schoepfer, S.D., Shen, J., Wei, H., Tyson, R.V., Ingall, E., Algeo, T.J., 2015. Total organic carbon, organic phosphorus, and biogenic barium fluxes as proxies for paleomarine productivity. *Earth Sci. Rev.* 149, 23–52.
- Seifert, W.K., Moldowan, J.M., 1986. Use of biological markers in petroleum exploration. In: Johns, R.B. (Ed.), *Methods in Geochemistry and Geophysics*, vol. 24, pp. 261–290.
- Shen, J., Schoepfer, S.D., Feng, Q., Zhou, L., Yu, J., Song, H., Wei, H., Algeo, T.J., 2015. Marine productivity changes during the end-Permian crisis and Early Triassic recovery. *Earth-Science Reviews. Global review of the Permian-Triassic mass extinction and subsequent recovery: Part II* 149, 136–162.
- Shi, Z.S., Chen, K.Y., Shi, J., Liu, B.J., He, H.J., Liu, G., 2003. Feasibility analysis of the application of the ratio of strontium to barium on the identifying sedimentary environment. *Fault-Block Oil Gas Field* 10, 12–16 (in Chinese with English abstract).
- Shields, G., Stille, P., 2001. Diagenetic constraints on the use of cerium anomalies as palaeoseawater redox proxies: an isotopic and ree study of cambrian phosphorites. *Chem. Geol.* 175, 29–48.
- Suttner, L.J., Dutta, P.K., 1986. Alluvial sandstone composition and palaeoclimate. 1. Framework mineralogy. *J. Sediment. Petrol.* 56, 329–345.
- Talbot, M.R., 1988. The origins of lacustrine oil source rocks: evidence from the lakes of tropical Africa. *Geological Society, London, Special Publications* 40, 29–43.
- Tao, S., Tang, D., Xu, H., Liang, J., Shi, X., 2013. Organic geochemistry and elements distribution in dahuangshan oil shale, southern junggar basin: origin of organic matter and depositional environment. *Int. J. Coal Geol.* 115, 41–51.
- Taylor, S.R., McLennan, S.M., 1985. *The Continental Crust: its Composition and Evolution*. Oxford, Blackwell, pp. 57–72.
- Ten Haven, H., De Leeuw, J., Rullkotter, J., Damsté, J.S., 1987. Restricted utility of the pristane/phytane ratio as a palaeoenvironmental indicator. *Nature* 330, 641–643.
- Tenger, T., Liu, W.H., Xu, Y.C., 2006. Comprehensive geochemical identification of highly evolved marine hydrocarbon source rocks: organic matter, palaeoenvironment and development of effective hydrocarbon source rocks. *Chinese J. Geochem. (Tokyo)* 25, 332–339.

- Tian, S.G., Niu, S.W., Pang, Q.Q., 2008. Redefinition of the lower cretaceous terrestrial yixianian stage and its stratotype candidate in the Luanping Basin, northern Hebei, China. *Geol. Bull. China* 27, 739–752 (in Chinese with English abstract).
- Tissot, B., Durand, B., Espitalie, J., Combaz, A., 1974. Influence of nature and diagenesis of organic matter in formation of petroleum. *AAPG Bull.* 58, 499–506.
- Tissot, B.P., Welte, D.H., 1984. *Petroleum Formation and Occurrence*. Springer Verlag, Berlin.
- Tyson, R.V., 2005. The “productivity versus preservation” controversy: cause, flaws, and resolution. *Special Publication-SEPM* 82, 17–33.
- Van Krevelen, D., 1961. *Coal: Typology*. Chemistry, Physics, Constitution. Elsevier Publishing Company, New York.
- Walker, C.T., Price, N.B., 1963. Departure curves for computing paleosalinity from boron in illites and shales. *AAPG Bull.* 47, 833–841.
- Wang, W.C., Xu, Y.C., Schidlowski, M., Faber, E., Stahl, W., 1997. The geochemical characteristics of carbon and hydrogen isotopes of kerogens of various maturity and depositional environments. *Acta Sedimentol. Sin.* 15, 133–137.
- Wang, Z., Fu, X., Feng, X., Song, C., Wang, D., Chen, W., Zeng, S., 2015. Geochemical features of the black shales from the Wuyu Basin, southern Tibet: implications for palaeoenvironment and palaeoclimate. *Geol. J.* 52, 282–297.
- Wei, C., Dong, T., He, Z., He, S., He, Q., Yang, R., Guo, X., Hou, Y., 2021. Major, trace-elemental and sedimentological characterization of the upper Ordovician Wufeng-lower Silurian Longmaxi formations, Sichuan Basin, south China: insights into the effect of relative sea-level fluctuations on organic matter accumulation in shales. *Mar. Petrol. Geol.* 126, 104905.
- Worash, G., 2002. Geochemistry provenance and tectonic Subunitting of the Adigrat sandstone northern Ethiopia. *J. Afr. Earth Sci.* 35, 185–198.
- Wright, J., Schrader, H., Holser, W.T., 1987. Paleoredox variations in ancient oceans recorded by rare earth elements in fossil apatite[J]. *Geochem. Cosmochim. Acta* 51 (3), 631–644.
- Wu, F.D., Chen, Y.J., Hou, Y.A., Zhang, F., Li, Y., 2004. Characteristics of Sedimentary–Tectonic Evolution and High-Resolution Sequence Stratigraphy in Luanping Basin, vol. 29. *Earth Science-Journal of China University of Geosciences*, pp. 625–630 (in Chinese with English abstract).
- Xi, D.P., Wan, X.Q., Jansa, L., Zhang, Y.Y., 2011. Late Cretaceous palaeoenvironment and lake level fluctuation in the Songliao Basin, northeastern China. *Isl. Arc* 20, 6–22.
- Xing, L., Lockley, M.G., Qin, Z., Klein, H., Romilio, A., Persons, W.S., Nie, X., Wan, X., 2019. Dinosaur tracks from the lower cretaceous Xiguayuan Formation in the Luanping Basin, Hebei province, China. *Cretac. Res.* 103, 104163.
- Xiong, Y.Q., Zhang, H.Z., Geng, A.S., 2004. Variation of carbon isotopic composition of kerogen during thermal evolution. *Petroleum Geology and Experiment* 26, 484–487 (in Chinese with English abstract).
- Yan, D., Xu, H., Xu, Z., Lei, Z., Tian, M., Cheng, L., Ma, Y., Wang, Z., Ostadhassan, M., 2020. Sedimentary architecture of hyperpycnal flow deposits: cretaceous sangyuan outcrop, from the Luanping Basin, north east China. *Mar. Petrol. Geol.* 121, 104593.
- Yuan, X., Jiang, Z., Zhang, Y., Jiang, H., 2020. Characteristics of the Cretaceous continental shale oil reservoirs in Luanping Basin. *Acta Petrol. Sin.* 41, 1197–1208.
- Zhang, M., Wengao, L., Jun, X., 1985. The discovery of halophilic algae and halobacteria at Zabuye Salt Lake Tibet and preliminary study on the geocology. *Acta Geol. Sin.* 2, 162–171 (in Chinese with English abstract).
- Zhang, Y., Yuan, X., Wang, M., Ge, P., Huo, Y., Xu, J., Zhang, J., Cheng, J., Jiang, Z., 2021. Discovery of lacustrine shale deposits in the Yanshan Orogenic Belt, China: implications for hydrocarbon exploration. *Geosci. Front* 12, 101256.
- Zhang, Y.L., Qu, H.J., Meng, Q.R., 2007. Depositional process and evolution of luanping early cretaceous basin in the yanshan structural belt. *Acta Petrol. Sin.* 23, 667–678 (in Chinese with English abstract).
- Zhao, Z.Y., Zhao, J.H., Wang, H.J., Liao, J.D., Liu, C.M., 2007. Distribution characteristics and applications of trace elements in Junggar Basin. *Natural Gas Exploration and Development* 30, 30–33 (in Chinese with English abstract).